Wear 408–409 (2018) 248–273

Contents lists available at ScienceDirect

Wear

journal homepage: www.elsevier.com/locate/wear

Slurry erosion of steel – Review of tests, mechanisms and materials

Vahid Javaheri[a,*], David Porter[a], Veli-Tapani Kuokkala[b]

[a] Department of Material Engineering and Production Technology, University of Oulu, P.O. Box 4200, Finland
[b] Department of Material Science, Tampere University of Technology, P.O.B 589, Finland

ARTICLE INFO

Keywords:
Slurry
Erosion
Pipeline
Erosion test
Erosion mechanism

ABSTRACT

Slurry erosion is a severe problem and a major concern for slurry handling equipment, as it leads to considerable expense caused by failures, downtime and material replacement costs. Slurry erosion is dependent on several parameters such as slurry properties, service conditions, and material properties. Hence, much high-quality research has been aimed at obtaining a fundamental understanding of this complex failure mode and developing new test methodologies and erosion resistant materials to minimize erosion rates. This is a review of the literature covering research into the effects of the main parameters influencing the slurry erosion of different types of steels, focusing on those which have been developed for pipeline applications. The types of bench-scale erosion test rigs, the mechanisms involved, and the behavior of different microstructures under slurry erosion conditions are discussed.

1. Introduction

Recently, slurry erosion caused by solid particles has received considerable attention amongst researchers, owing to the intensity of the problems it causes to equipment in service, especially for short- and long-distance pipeline systems used for the transportation of slurries containing ores or tailings in mining operations, or oil and gas transportation in the power generation industry.

Erosion-related problems cause serious financial losses in these industries. Any failure of a pipeline component results in expensive repairs, loss of production time, or possibly harmful environmental effects. Since failure is usually not predictable due to variable operating conditions, methods for reducing the erosion and increasing the lifetime of the pipe including the development of new steels for pipeline systems are of interest to these industries. The erosion rate of a slurry pipeline depends on various factors such as slurry and solid particle properties, flow rate, and pipeline material. The most popular way to study the effect of the influencing variables and to understand the erosion mechanisms is to conduct investigations using laboratory equipment, i.e. bench-scale test rigs.

Erosion, abrasion, and corrosion are the main types of damage mechanisms taking place in slurry equipment and hydraulic components, the main one being erosion [1–4]. Slurry erosion is a complex phenomenon which was systematically investigated for the first time by Finnie [5] and Bitter [6] in the 1960s. Since then much research has been conducted on the assessment of erosion using various evaluation techniques and test methods.

In order to develop solutions to minimize the effects of erosion, it is essential to have a fundamental and comprehensive understanding of the erosion and tribological mechanisms involved. Hence, the purpose of this work is to provide a comprehensive review of the literature concerning the slurry erosion of steels, especially those that have been developed for pipeline applications. The types of erosion bench-scale test rigs, the mechanisms involved, proposed models and the parameters affecting the erosion rate in different steel microstructures are discussed. It must be emphasized that, despite the possible synergetic effects of erosion and corrosion [7,8], this review has been limited to erosion only; other wear mechanisms such as abrasion, corrosion or cavitation erosion are not covered.

2. Theoretical background

2.1. Types of slurry

A slurry is generally defined as a heterogeneous mixture of a fluid, i.e. a gas or a liquid, here mostly liquid, and one or more kinds of solid particles varying in size from a few microns to a few millimeters [9]. Owing to the high particle concentration, a slurry can sometimes be classified as a highly viscous fluid. The most important characteristics of slurries are defined by their rheology. The rheology is a dynamic property of the microstructure of the slurry, which is affected by various factors such as the shape, size, density and mass fraction of the suspended solid particles and the viscosity and density of the carrier fluid [10]. Slurries could be categorized into two general types: settling

* Corresponding author.
E-mail addresses: Vahid.Javaheri@oulu.fi (V. Javaheri), David.Porter@oulu.fi (D. Porter), Veli-Tapani.Kuokkala@tut.fi (V.-T. Kuokkala).

https://doi.org/10.1016/j.wear.2018.05.010
Received 17 July 2017; Received in revised form 8 May 2018; Accepted 9 May 2018

Nomenclature

a, b, c, e	equation constant
A_i	equation constant
A_P	projected particle impact area
A_{Pipe}	pipe cross-sectional area
B	material dependent exponent
C	equation coefficient
C_0	volume of delivered slurry
$C_{avg.}$	mean slurry concentration
C_K	cutting characteristic velocity
C_W	slurry concentration
$C_{w,k}$	slurry concentration of the specific particle class size of K
d′	particle diameter experimental constant
d_i	the average particle diameter of two consecutive sieve sizes
d_P	particle size (diameter)
$d_{P,W}$	mass-weighted mean particle size
$\frac{dr}{dt}$	velocity of surrounding slurry
$\frac{d_{rp}}{dt}$	radial particle velocity
$\frac{d_y}{dt}$	normal particle velocity
D	equation coefficient
D_K	deformation characteristic velocity
D_P	pipe diameter
e_T	elongation of target material
E_{90}	erosion damage at normal impact
E_α	angular dependence of erosion damage
E_C	cutting component of the erosion damage
E_D	deformation component of the erosion damage
E_P	elastic modulus of target material
E_S	specific energy
$E_{S,k}$	specific energy of particulate species k
E_t	elastic modulus of target material
E_T	total erosion rate
E_T^{max}	maximum erosion rate
f(α)	erosion impact angle dependence function
$f(\alpha_k, d_{P,k})$	specific energy coefficient
f	fraction of volume loss caused by the median spalling
f_i	the fraction of each specific particle size in a multi-size particle slurry
f_l	volume fraction of liquid flow
$F_{cent.}$	centrifugal force
$F_{d,V}$	degree of particle fragmentation
F_{dr}	drag force
F_e	specific erosion factor
h	erosion depth
H_{ch}	height of channel
H_P	particle hardness
H_T	target material hardness
i	material dependent exponent
k_1	hardness exponent in the erosion equations
K	empirical constant
K_i (i = 1–4)	equation constant
K_T	target material toughness
l_p	particle displacement
L_P	particle length
m	particle velocity exponent in the erosion equations
M_P	mass of the impacting particle
MS_F	modified particle shape factor
n	particle size exponent in the erosion equations
n_i (i = 1–4)	equation constants
N_P	number of particles throughput
p	slurry concentration exponent in the erosion equations
P_n	function of material work hardening properties
P_t	function of material plastic flow stress
P	projected particle impact perimeter
P_F	friction power per unit area
P_{TR}	particle tangential restitution ratio
q_p	flow rate of solid particles
Q	volumetric flow rate
r	instantaneous location of liquid unit
r_p	instantaneous location of particle
r_P	particle radius
R_{Ch}	mean Coriolis channel radius
Re_H	reynold number (for average inlet velocities) for the channel height of H_{ch}
R_f	particle roundness factor
S_F	particle shape factor
$(S_F)_{Avg}$	mean particle shape factor
$(S_F)_{Max}$	maximum particle shape factor
$(S_F)_{Min}$	minimum particle shape factor
S_T	stiffness of target material
t	erosion time
u_P	tangential velocity of the solid particles
$u_{P,k}$	tangential velocity of particulate species k
v'	standard impact velocity experimental component
v_*	friction velocity
v_f^z	velocity of fluid in the axial direction
V_m	mean velocity
v_p^r	velocity of particle in the radial direction
v_p^z	velocity of particle in the axial direction
v_{pt}^r	impact velocity in the radial direction
V	volume of removed material
V_N	particle normal velocity
V_P	particle velocity
$V_{P,k}$	velocity of the specific particle class size of K
V_{Ref}	reference particle velocity
V_{SL}	superficial liquid velocity
V_T	particle tangential velocity
W^{-1}	erosive-abrasive wear resistance
W_0	proportion of the particle (by weight) within the specified particle size range before test
W_1	proportion of the particle (by weight) within the specified particle size range after test
W	passage width
W_I	impact erosive wear
W_P	particle width
W_s	sliding erosive wear
Y_s	yield stress

Greek letters

α_1	angle at which erosion experimentaly starts
α	particle impact angle
α_m	angle of maximum erosion
δ	boundary layer thickness
$\widehat{\varepsilon_1}$	maximum erosion for the reference velocity of primary erosion
$\widehat{\varepsilon_2}$	maximum erosion for the reference velocity of secondary erosion
ε	empirical constant
ε_{Cr}	critical strain
η	erosion efficiency
η_δ	attenuation coefficient
ν_P	Poisson's ratio of particle
ν_T	Poisson's ratio of target material
ξ	erosion mechanism identifier
ρ_L	density of carrier liquid
ρ_P	particle density
$\rho_{P,k}$	density of the specific particle class size of K

ρ_T	target material density	φ	empirical constant
σ_{cr}	critical stress	Φ	particle kinetic energy
τ	shear stress between the eroded surface and particulate phase	ω	rotational (angular) rotor velocity
τ_k	shear stress of particulate species k	ω_H	rotational velocity for the channel height of H_{ch}

and non-settling slurries depending on the size of the solid particles. In non-settling slurries, the tendency of the solid particles to settle out from the carrier liquid is low because the particles are sufficiently fine, light or concentrated, while in settling slurries this is not the case and the tendency to settle out needs to be taken into account in the design of the slurry transportation system or developing related models [10].

2.2. Slurry erosion

Particulate slurry transportation can involve abrasion, erosion and corrosion [11,12]. Among these, erosion accounts for the largest share of the total wear and material removal. Erosion is a process of wear which is defined as the progressive loss, fracture or displacement of material under the repeated impingement of solid particles on a particular solid surface. In other words, the process of metal removal from a surface due to the impact of erodent particles on the surface is considered as erosion [13]. Slurry erosion usually occurs under turbulent flow conditions when the moving slurry strikes a surface, scars it and removes material. It has to be remarked that as erosion and abrasion are both mechanical wear processes showing many similarities [14], they are sometimes confused with each other. However, the basic difference between the two is that erosion involves a transfer of kinetic energy from the impinging particle to the target surface, whereas abrasion is the loss of material due to the passage of hard particles over the surface without impingement, as schematically shown in Fig. 1. In erosion, the contact time between the erodent and the eroded surface is much shorter than in abrasion [15].

2.3. Mechanisms of erosion by solid particles

Slurry erosion is a complex, time dependent phenomenon which is not yet fully understood. The phenomenon is complicated by the interaction of many parameters such as erosive particle characteristics, eroded material properties, operating conditions and the different erosion mechanisms. It is generally assumed that erosion, regardless the material ductility or brittleness, occurs due to two main mechanisms, referred to as “cutting” and “deformation” originally defined by Finnie [5]. It has to be noted that *cutting* and *deformation* are just terms which were initially selected to describe these mechanisms and that have since become established through frequent use. They do not mean exactly what the words *cutting* and *deformation* are usually understood to mean metallurgically, especially in the case of brittle materials including brittle (i.e. not ductile) steel. Thus, they are not really suitable terms and may be the cause of confusion. Nonetheless, the *cutting mechanism* is associated with particles impacting the eroding surface at an oblique angle with sufficient energy to gouge a fragment loose while the *deformation mechanism* is associated with particles impacting perpendicular to the eroding surface with enough kinetic energy to cause plastic deformation or subsurface crack formation in the eroding material surface, i.e. stresses higher than the yield strength, and eventual failure [17]. These two mechanisms for both ductile and brittle materials are illustrated in Fig. 2.

Accordingly, on the basis of the previous works by Finnie [5] and Bitter [6], Clark and Wong [17] proposed that the total erosion (E_T) occurring in unit time could be expressed as the sum of the deformation (E_D) and cutting erosion (E_C) mechanisms by the following simplified equations:

$$E_T = E_C + E_D \tag{1}$$

$$E_T = \frac{1/2M_P(V_N{}^2)}{\varepsilon} + \frac{1/2M_P(V_T{}^2\sin 2\alpha)}{\varphi} \tag{2}$$

where M_P is the total mass of uniformly sized impacting particles, V_T and V_N are, respectively, the values of the tangential and normal velocity components of the particle at the impact angle α. ε and φ are empirical constants which are related to the specific energy for deformation erosion and the unit of kinetic energy for cutting erosion, respectively. They depend on the test conditions and need to be determined experimentally. For instance, the value of ε can be evaluated at the impact angle 90° where only deformation erosion takes place and then φ evaluated from experiments at oblique angles when ε for that experimental condition is known. A rough estimate of φ can be obtained from the particle velocity, density and dimension as shown later in Section 3.2.1 (Eq. (11)). A schematic illustration of Eq. (2) is given in Fig. 3.

Apart from the impact angle, the contribution of each mechanism to the total erosion also depends on the ductility of the target surface as reported by many authors [5,19–21]. From this point of view, erosion is broadly divided into *ductile erosion* and *brittle erosion*. Ductile erosion with oblique impact involves material removal by cutting/ploughing while ductile erosion under normal impact involves the formation of a crater with extruded lips and consequent ductile fracture. Brittle erosion occurs by the formation and intersection of a network of subsurface cracks. A combination of erosion mechanisms and modes can operate simultaneously, although, depending on the impact conditions and material properties, one may predominate. Extending the role of particle impact angle on erosion further, Islam [22] suggested that the main mechanisms could be classified according to different

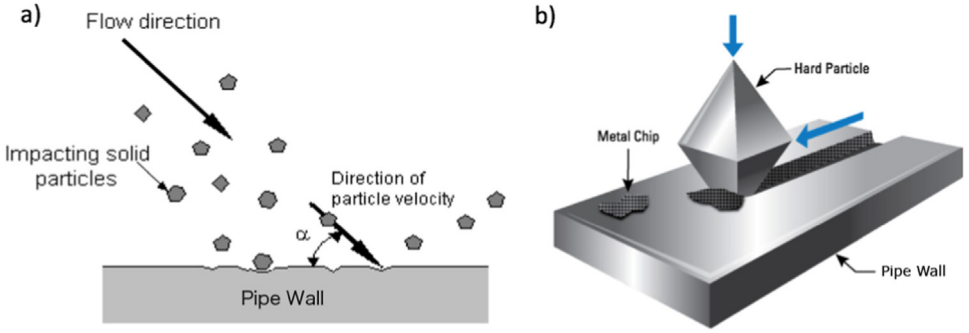

Fig. 1. Schematic diagram of a) solid particle erosion under turbulent flow condition [15] and b) abrasion under laminar flow condition [16].

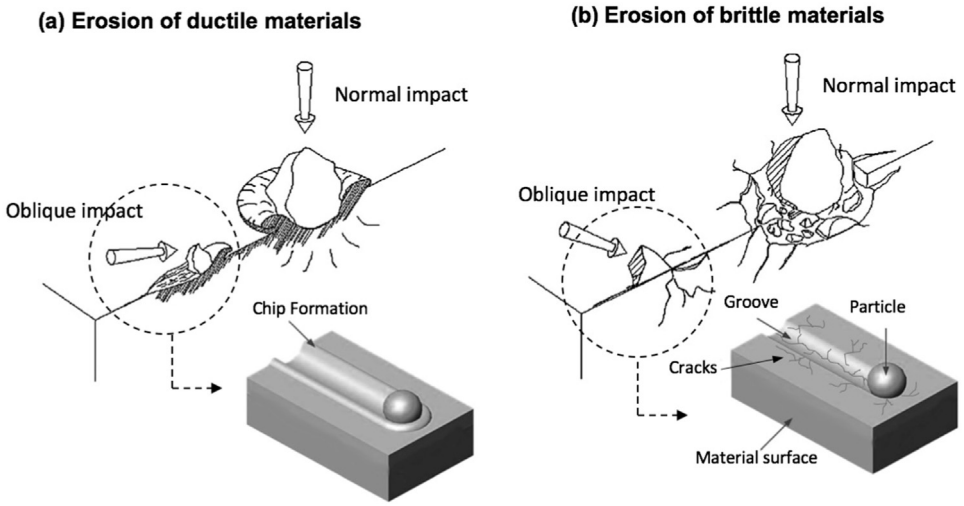

Fig. 2. Schematic representation of erosion caused by deformation mechanism at normal impact and cutting mechanism at oblique impact in a) ductile and b) brittle materials [18].

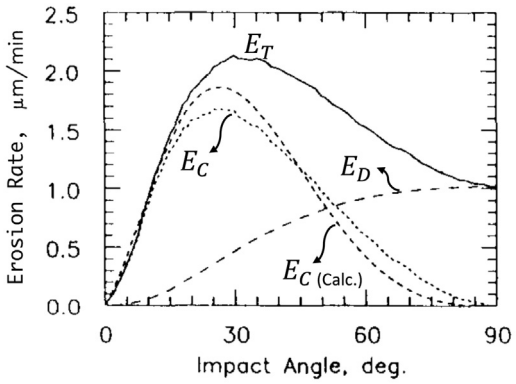

Fig. 3. Graphical representation of total erosion, E_T (solid line) as a function of deformation component, E_D (long-dash line) and derived cutting component of erosion, E_C (dotted line) and calculated cutting component of erosion, $E_{C(calc.)}$ (short-dash line for hot rolled 1020 steel eroded by 463 μm SiC at 18.7 m/s in diesel oil [17].

combinations of the particle impact angle and particle velocity as described below for the steel API X42 (0.28C, 1.30Mn, and 0.15Si wt%).

Low impact angle and low particle velocity

As the particles slide on the surface, they squeeze the metal ahead and to the sides to form ridges. Therefore, under these conditions, ploughing is the dominant erosion mechanism. To discriminate between ploughing and cutting it should be noted that in ploughing, the material is not removed from the surface and just shifts to the side of the erosion groove [23]. While, in cutting a debris forms in front of the erosive particle and a volume of material equal to the volume of the erosion groove is lost from the surface, as illustrated in Fig. 4.

Low impact angle and high particle velocity

Under these conditions, cutting is the main mechanism of erosion. Nevertheless, material removal also occurs by the fracture of ridges, particularly, at the later stages of the erosion process where, owing to repeated energetic particle impact, the work-hardened surface is partly brittle and ready to crack and fracture, as shown in Fig. 5.

High impact angle and low particle velocity

Under these conditions, plastic deformation and flattening of ridges is the main mechanism, as schematically illustrated in Fig. 6, where repeated impact by the abrasive particle causes fracture and removal of vulnerable lips [24].

High impact angle and high particle velocity

Particle fracture and secondary metal cutting constitute a large share of the total erosion for high impact angle and high particle velocity. Erosive particles strike and are deflected by previously embedded particles resulting in the removal of a small metal particle, ca. 2–3 μm in length. The secondary cutting is demonstrated in Fig. 7.

It should be noted that the above categorization of erosion mechanisms is not absolute and a combination of them can take place at the same time. In order to identify the dominant mechanism leading to solid particle erosion, a new parameter was introduced by Sundararajan et al. [25]. They proposed that the ratio of the eroded material volume to the volume of the craters formed could be presented as an erosion efficiency parameter (η). By considering the erosion rate in terms of volume lost per unit mass of the erodent, it can be simplified as

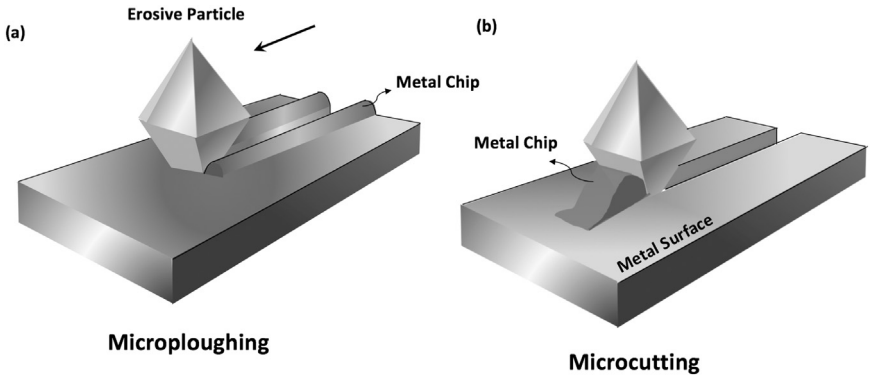

Fig. 4. Schematic illustration of a) microploughing and b) microcutting erosion mechanism.

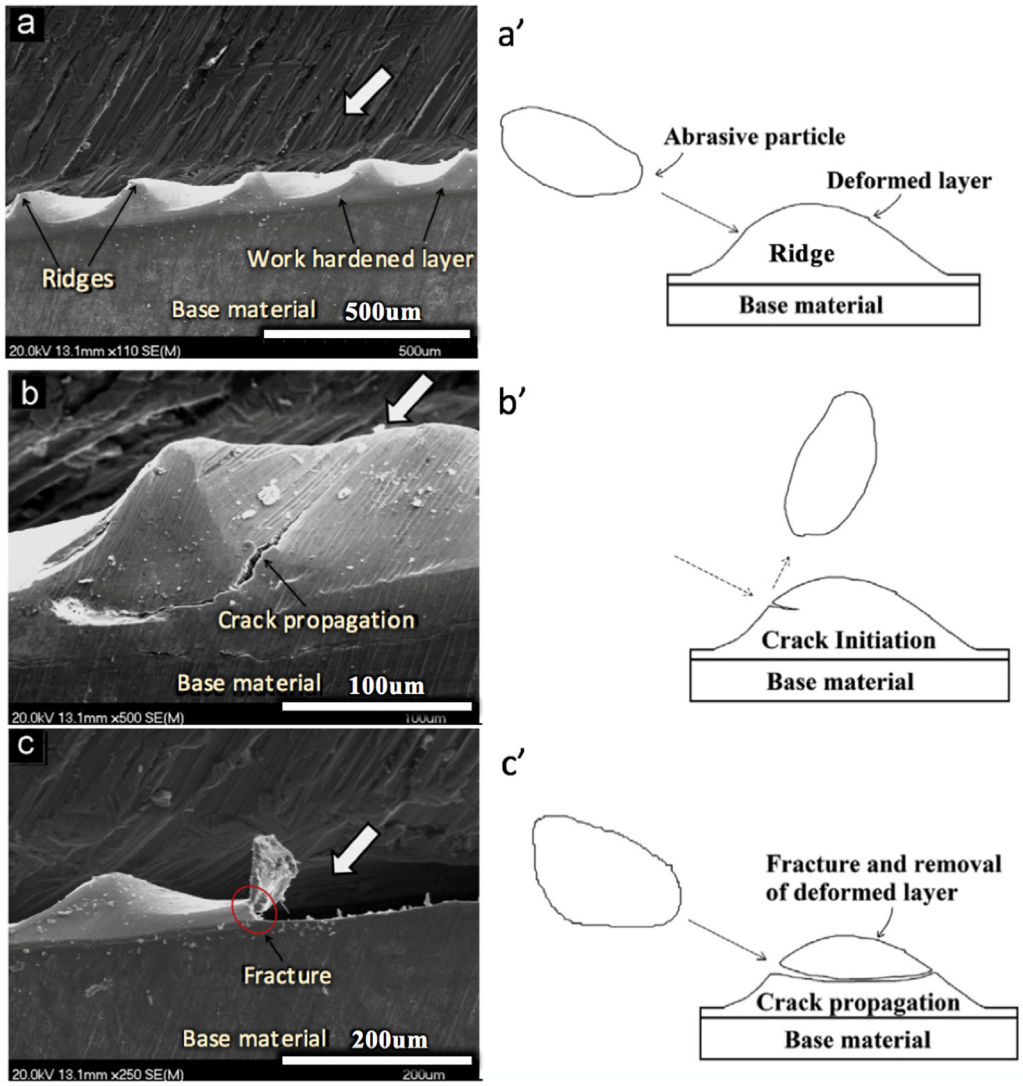

Fig. 5. a–c) SEM micrograph of the cross-sectioned layers of an erosion scar. White arrows indicate particle flow direction. (a) Eroded and deformed layer, (b) sub-surface crack propagation, (c) fracture of the deformed layer. a´–c´) Schematic illustrations of the metal removal steps [22]. (Erosion test: A sand blast type tester with aluminum oxide particles).

$$\eta = \frac{2H_T V}{M_P V_P^2} \tag{3}$$

where H_T is the hardness of the target material (HV), V is the volume of removed material (m^3), and M_P (kg) and V_P (m/s) are the mass and velocity of the particle, respectively. In the case of normal impact erosion, it has been suggested that the brittle mechanism is dominant when $\eta > 1$, whereas deformation controls the erosion mechanism if $\eta < 1$.

Later, Grewal and co-workers [26], by considering the required and expended energy for the material removal, extended Eq. (3) and introduced an *erosion mechanism identifier* (ξ) for prediction of the erosion mechanism under both oblique and normal impact.

$$\xi = \frac{2V\sigma_{cr}\left(\frac{H_T}{K_T}\right)}{M_P V_P^2} \tag{4}$$

where V, H_T, M_P, and V_P have the same meanings as in Eq. (3); K_T is a material toughness (MPa) and σ_{cr} is a critical stress (MPa) dependent on the type of material. For brittle metals and alloys, σ_{cr} is considered to be equal to the ultimate tensile strength whereas for ductile materials, σ_{cr} is taken as equivalent to the ultimate shear stress. The ultimate shear strength of steel could be roughly estimated as approximately 75% of the ultimate tensile strength. It was proposed that the dominant erosion

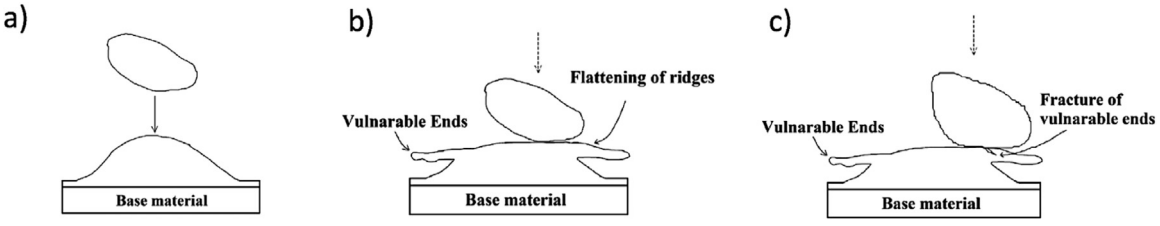

Fig. 6. Schematic illustration of the metal removal steps at low velocity and high impact angle [22].

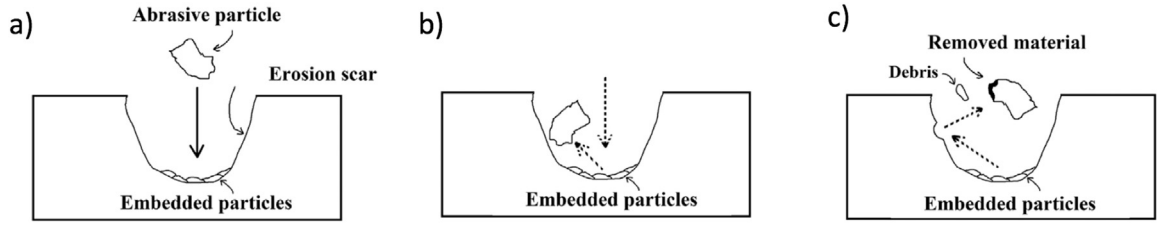

Fig. 7. Schematic illustration of the secondary cutting process steps at high velocity and high impact angle [22].

mode is ploughing if $\xi < 1$, microcutting if $\xi = 1$, and brittle if $\xi > 1$.

3. Parameters affecting slurry erosion

Several researchers have measured and quantified the effect of different parameters on solid particle slurry erosion. The parameters can be classified into four groups, i.e. the nature of the target surface, the nature of the erosive particles, the characteristics of the flowing slurry, and the contact or impingement condition. These are presented in a typical cause-and-effect (fish bone) diagram in Fig. 8. The parameters in bold in Fig. 8 are discussed below.

3.1. Particle properties

3.1.1. Particle shape

Many attempts have been made to correlate slurry erosion with various characteristics of the erodent particles such as shape, size, density and hardness [27–31]. The major part of this research has been focused on the particle shape as one of the most significant factors influencing slurry erosion. For this purpose, several types of erodents have been employed to make the test condition as close as possible to real conditions [32,33]. Some properties of the most commonly used particles are presented in Table 1 and Fig. 9. Note that concentrate and ore are typical raw materials in the metallurgical industry, matte is an intermediate product in metallurgical processing, tailings are left when all the valuable metals have been extracted, and steel shot and grits are steel abrasive particles used in shot blast cleaning or surface preparation of industrial parts.

Other things being equal, it is obvious that angular sharp particles will cause more erosion than spherical particles. Initially, Levy and Chik [32] reported that sharp angular sand particles caused a four-fold increase in erosion when compared to spherical particles.

As early as 1927, to quantify the effect of particle shape on the erosion, Cox [42] quantified the effect of particle shape on erosion by defining the particle circularity through the shape factor (S_F) given by:

Table 1
Properties of frequently used erodent particles.

Erodent particles	Hardness (HV)	Specific gravity (g cm^{-3})	Shape	Ref.
Alumina (Al_2O_3)	1800	3.94	Angular	Desale [34]
Silicon Carbide (SiC)	2500	3.22	Angular	Desale [34]
Quartz (SiO_2/ Silica sand)	750	2.65	Fairly rounded	Clark [35]
Glass Beads	600	2.6*	Spherical	Arabnejad [36] *Oka [37]
Steel Round Grits	–	–	Spherical	Vite-Torres [38]
Chromite	–	4.05	–	Lindgren [39]
Matte	–	4.72	–	Lindgren [39]
Concentrate	–	3.43	–	Lindgren [39]
Tailings	–	2.89	–	Lindgren [39]
Mining Ore	–	4.62	–	Lindgren [39]
Steel Shot	880	7.89	Spherical	Yabuki [40]
Brass Shot	210	8.43	Angular	Yabuki [40]
Tungsten Carbide	2200	15.7	Irregular	Feng [41]
Diamond	8000	3.5	Blocky	Feng [41]

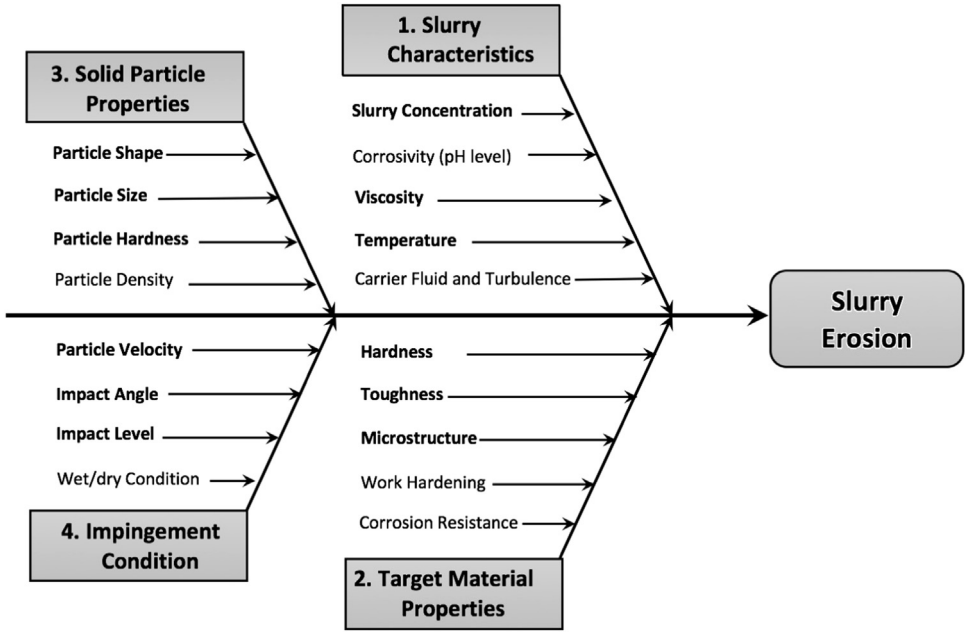

Fig. 8. Important parameters influencing slurry erosion.

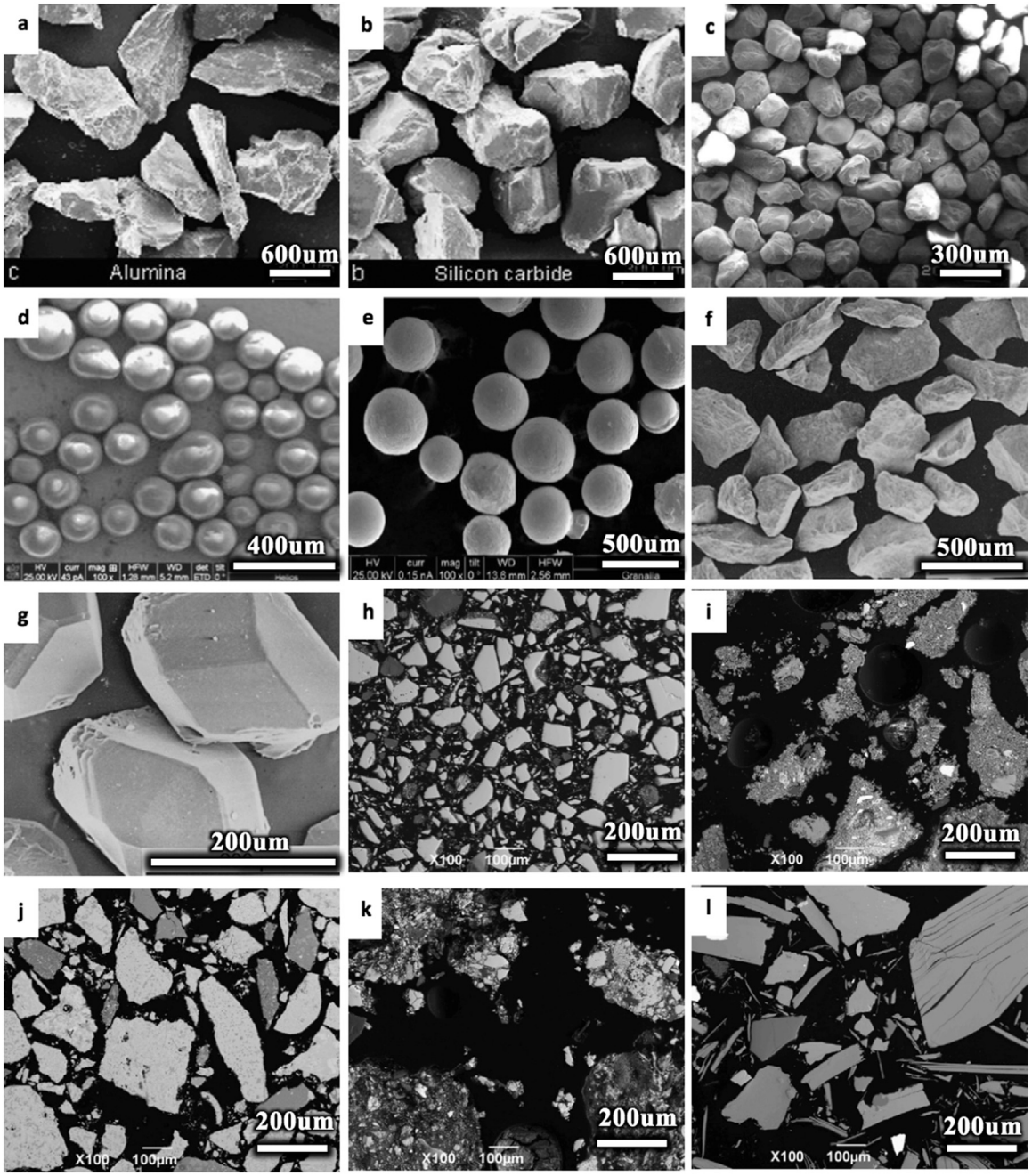

Fig. 9. SEM images of a) alumina [34], b) silicon carbide [34], c) quartz [35], d) glass beads [36], e) steel round grit [38] f) tungsten carbide [41], g) diamond [41] and cross-section SEM images of h) chromite, i) concentrate, j) matte, k) ore, and l) tailings [39]. Note magnifications differ.

$$S_F = \frac{4\pi A_P}{P^2} \tag{5}$$

where, A_P is the projected impact area (m^2) and P is the overall perimeter (m) of the projection of a solid particle. The particle perimeter can be also calculated on the basis of the measured length (L_P) and width (W_P) of the particle as given in Eq. (6) [43]:

$$P = \frac{\pi}{2}\left[\frac{3}{2}(L_P + W_P) - (L_P/w_P)^{1/2}\right] \tag{6}$$

For a circular particle, the shape factor is equal to unity and any deviation away from unity indicates a departure from circularity. Thus, the lower the value of the shape factor, the higher the angularity of the particles.

Because of the high standard deviation observed for many particle measurements, Voort [44] modified the shape factor equation as follows:

$$MS_F = [(S_F)_{Avg}(S_F)_{Min}(S_F)_{Max}]^{1/3} \tag{7}$$

where $(S_F)_{Avg}$ is the average of all measurements, and $(S_F)_{Min}$ and $(S_F)_{Max}$ are the minimum and maximum values of S_F.

3.1.2. Particle size

Clearly, on a per particle basis, big particles accelerate slurry erosion over that of small ones. Apart from the fact that smaller particles are more likely to remain suspended in the slurry flow and not strike the surface, when impacting the surface, larger particles transfer more kinetic energy to the target surface and cause greater erosion per impact [16,19]. Many investigators [17,27,32,41,45–48] have reported that there is a power-law dependence of erosion rate on particle size, i.e.

$$Erosion\ rate \propto (Particle\ size)^n \tag{8}$$

The value of the exponent 'n' has been reported to vary in the range of 0.2–4.0. Gandhi and Borse [49] showed that to be more precise, for the fine particulate slurries, it is better to consider the mean size of the particles as the particle size, whereas the weighted-mass particle size ($d_{P,W}$), obtained from screening with different sieve sizes, is a better choice for multi-sized particulate slurries. The weighted-mass particle size is calculated by considering the particle volume to be proportional to the cube of one of its linear dimensions as follows:

$$d_{P,W} = \left\{\sum_{i=1}^{N} f_i d_i^3\right\}^{1/3} \tag{9}$$

where N is the number of size groups into which the total sample is divided, f_i the fraction of solids in each size group, d_i the average diameter of two consecutive sieve sizes, i.e. the sieve on which the solids are retained and the previous one.

3.1.3. Erodent and target hardness

Generally, with an increase in the ratio of the erodent particle hardness to the hardness of the target material, the total erosion increases until a certain value after which a further rise in the hardness ratio has little effect. Levi and Chik [32], by erosion testing of cold rolled steel AISI 1020 with a hardness of 150 kgf mm^{-2} using particles with a range of hardness levels, i.e. calcite, apatite, sand, alumina and silicon carbide, showed that above a particle hardness of 700 kgf mm^{-2}, the erosion rate remained essentially constant, see Fig. 10.

Also, it is generally believed that materials with higher hardness have higher erosion resistance. For example, Divakar et al. [50] changed the hardness of AISI 316 steel by cold rolling and case hardening and showed that an increase in the hardness decreases the total erosion in a jet erosion tester. However, the toughness of the target material may complicate the correlation between erosion rate and hardness, since the loss of ductility generally accompanying an increase in hardness may increase the erosion rate through a brittle mechanism [51,52]. In the other words, if two materials have the same hardness value, the tougher may offer better erosion resistance under the same conditions.

3.2. Impingement condition

3.2.1. Particle velocity

Erosion increases with an increase in the slurry particle (flow) velocity. Numerous researchers [14,20,24,53–56] have proposed that the erosion rate exhibits an empirical power law relationship with the erosive particle velocity:

$$E_T = KV_P^m \tag{10}$$

where E_T is the erosion rate, V_P is the velocity of the solid particles (m/s), K is an empirical constant, and m is the velocity exponent varying from 0.34 to 4.83 depending upon the particle and material properties and condition of the test [14,24]. For instance, Hutchings et al. [57] reported K = 5.82×10^{-10} and m = 2.9 a mild steel impacted obliquely by solid steel spheres.

Higher impingement velocity of course means higher kinetic energy leading to higher localized force and more erosion. If the particles are assumed to be spherical with a diameter d_P and density ρ_P travelling with a velocity of V_P, their kinetic energy Φ is simply given by [39]:

$$\Phi = \frac{\pi\rho_P d_P{}^3 V_P{}^2}{12} \tag{11}$$

Tilly [53] pointed out that big particles travelling at high velocity can break up on impact into the smaller particles. The fragmented particles either rebound from the surface or impact around the primary site causing radial damage. Hence, by considering a major role for the particle velocity and particle fragmentation, they proposed one of the earliest mechanistic erosion equations for ductile materials. A two-stage mechanistic relationship for the total erosion rate was suggested by introducing a standard test reference velocity (V_{Ref}) and threshold velocity (V_{tsh}) below which distortion is entirely elastic and no erosion occurs. The first stage occurs when the erosive particle strikes the target material and removes a chip from the surface. The second stage is caused by fragmented particles projected radially on the primary scars. For any impact angle, the total erosion rate, expressed as the material removed by unit mass of impacting particles, was suggested to be the sum of the two proposed stages, i.e.:

$$E_T = \widehat{\varepsilon_1}\left(\frac{V_P}{V_{Ref}}\right)^2\left[1-\left(\frac{d_{tsh}}{d_P}\right)^{3/2}\frac{V_{tsh}}{V_P}\right]^2 + \widehat{\varepsilon_2}\left(\frac{V_P}{V_{Ref}}\right)^2 F_{d,V} \tag{12}$$

where $\widehat{\varepsilon_1}$ and $\widehat{\varepsilon_2}$ are the maximum erosion (mg/g) for the reference velocity (m/s) of each stage; d_{tsh} is the threshold particle size (μm) below which no erosion damage occurs and $F_{d,V}$ is the degree of fragmentation, which is a function of particle size and velocity. It can be determined from the following:

$$F_{d,V} = \frac{W_0 - W_1}{W_0} \tag{13}$$

where W_0 and W_1 are the weight fractions of the particles within the specified particle size range before and after the test, respectively. If all the particles are fragmented into smaller particles, $F_{d,V}$ is equal to unity.

3.2.2. Particle impact angle

The impact angle, which is the angle between the direction of the particle velocity and the target surface, can also affect the amount of slurry erosion. The variation of erosion rate depends on the ductility of the target. In ductile materials, the maximum erosion occurs at intermediate impact angles. For instance, it has been reported [58] that for the steel AISI 1017 the maximum erosion rate has been observed at impact angles between 40° and 50° (Fig. 11a), while for brittle materials the maximum erosion rate occurs near normal impact, e.g. as with high-chromium white iron (Fig. 11b). Clearly, it is essential to take the target properties into account when choosing the function to describe the effect of impact angle in modeling or system design.

3.3. Slurry characteristics

3.3.1. Slurry concentration and viscosity

Many researchers, including Tsai et al. [59] and Gandhi and coworkers [47], have revealed that higher particle concentration in the slurry leads to a higher erosion rate due to the increasing number of particles that strike the wall surface. Indeed, viscous liquids increase the buoyancy of the solid particles keeping them suspended in the slurry flow. In the case of a slurry pipeline, in less viscous liquids, the solid particles tend to settle, forming a protective sliding bed at the bottom of the slurry pipeline [60]. This means that the metal loss

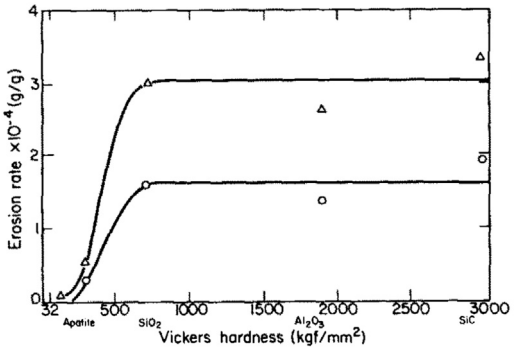

Fig. 10. Erosion rate of AISI 1020 steel by four erodents (given on the hardness axis) at two different impact angles: Δ = 30° and ◯ = 90° [32].

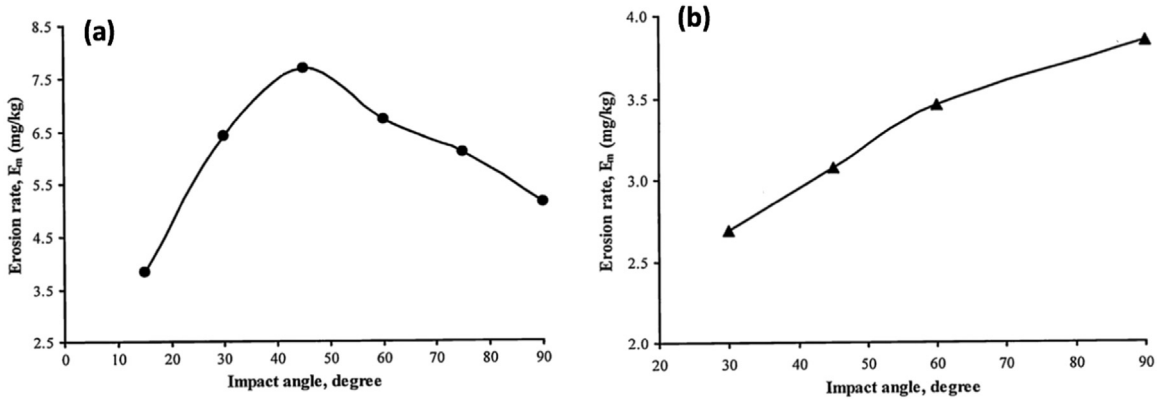

Fig. 11. Influence of impact angle on erosion rate in a whirling-arm test rig with silica particles impacting at 15 m/s. a) AISI 1017 steel (ductile material) and b) high-Cr white cast iron (brittle material) [58].

decreases with a decrease in the slurry viscosity. However, the effect of viscosity depends on the liquid velocity. Kesana et. al [61] reported that at low superficial velocities (18, 27, 35 m/s), metal loss increased with increasing liquid viscosity, while it decreased at high velocity (~ 45 m/s). Accordingly, Kowsari et al. [62] proposed that, at a very high velocity (110 m/s), an increase in viscosity causes a decrease in the erosion due to two viscous effects. First, the increased viscosity changes the stagnation zone and thereby reduces the particle impact energy and erosive ability. Secondly, the increased viscosity increases the particle momentum number, which decreases the local impact angle at the bottom of the eroded channel. Also, some researchers [63–65] believe that in the impinging jet erosion test, an increase in the slurry concentration can reduce the erosion rate owing to the increased efficiency of the higher viscosity fluid in removing particles away from the coupon surface after impact.

3.3.2. Slurry and surface temperature

The effect of temperature on the erosion rate depends on the system under consideration. Some researchers have shown that the erosion rate increases with increasing temperature. For example, Levy and Man [66] observed that the erosion rate of an alloy steel was about 6 times higher for a slurry temperature of 175 °C compared to 95 °C, which could be mainly attributed to a reduction in the kerosene fluid viscosity. Conversely, other researchers have found that by increasing the slurry and target surface temperature the erosion rate could be reduced. This was attributed to a higher ductility of the target surface at higher temperature resulting in more of the particle energy being absorbed by plastic deformation [67,68]. By using a commercial type of jet erosion tester on 304 austenitic stainless steel, Young and Ruff [69] showed that increasing the target material temperature from 25 °C to 500 °C caused a decrease in both the impingement angle at the erosion peak and the overall erosion rate as presented in Fig. 12. However, in the case of slurry transportation, operating temperatures do not vary greatly, so temperature effects are not expected to be important.

3.4. Target material properties

3.4.1. Microstructure

Target material properties are crucial factors with regard to the erosion rate and surface degradation in tribological systems [58]. Inhomogeneous target material properties arising from microstructural variations have been observed to lead to localized deformation by erosive particles even though the slurry flow is uniform. Therefore, there is an essential need to know more about the role of the target material and its microstructure in slurry erosion to assist in the selection of erosion resistant materials and to estimate the erosion damage in different applications.

According to the data reported by many researchers [18,35,70,71], the materials used in slurry erosion applications can be divided into two groups, brittle and ductile, depending on their hardness level, microstructure, and whether the maximum erosion rate occurs with normal impingement (often happens for the brittle material) or at impingement angles in the range of 30–50° (often happens for ductile materials) [58], as was already discussed in Sections 2.3 and 3.2.2. The classification of steels into these categories is reviewed in the following sections.

3.4.1.1. Ductile steels containing austenite, ferrite and pearlite microstructure. The slurry erosion rate of steels is significantly influenced by their microstructure, especially in the case of ductile steels, the microstructures consist of different phases with differing physical and mechanical characteristics. So, the mechanism of erosion depends on the response of the microstructure components to the erosion. This section reviews the erosion performance of various common ductile pipeline materials.

In aggressive erosion-corrosion conditions like those in hydrometallurgical processes, stainless steel pipe materials are often employed. Lindgren and Perolainen [39] studied the erosion resistance of two austenitic stainless steels (316L and 904L) and three ferritic - austenitic duplex stainless steels (LDX 2101, 2205, and 2507) by means of a slurry pot test for various erosion conditions covering several erodent materials and slurry concentrations. Their results showed that, on average, duplex grades exhibited higher erosion resistance than the austenitic grades. The reason for the better erosion resistance of the duplex microstructures was not only their higher surface hardness but also their higher yield strength which reduced plastic deformation. Therefore, in the duplex steels a smaller fraction of erodent particles had sufficient kinetic energy to initiate plastic deformation compared to the single-phase austenitic steel under the same erosion conditions. This

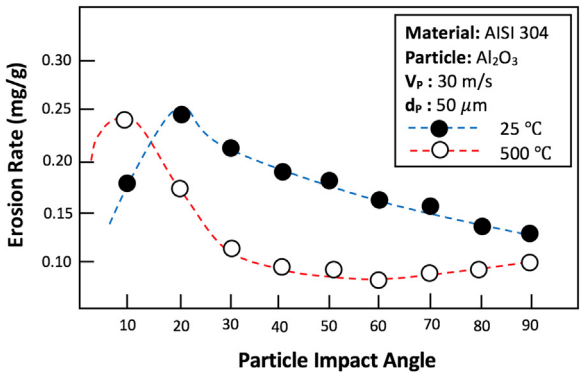

Fig. 12. Erosion rate of AISI 304 stainless steel in a commercial jet erosion tester with alumina erosive particles of 50 μm diameter and velocity of 30 m/s. Based on the results of Ref. [69].

was in line with Lindsley and Marder [72] and Ojala et al. [73] who showed that surface deformation could be an important aspect of the erosion mechanism in a single-phase steel.

Without doubt, low-carbon and medium-carbon steels with ferritic – pearlitic microstructures are the most common pipe materials in general application. By studying the erosion resistance of ferritic – pearlitic microstructures, Alam and co-workers [24] revealed that localized plastic deformation, flattening of pearlite plates, the formation of platelets and their subsequent removal by repeated impacts is one of the dominant degradation mechanisms of this kind of steel. By studying the response of two common ductile ferritic – pearlitic steel microstructures to different impact angles and impact velocities, they also showed that, during erosion, pearlite is more effective in resisting ploughing, cutting and deformation than ferrite [74]. AISI 1080, containing 100% pearlite with a hardness of 327 HB, and AISI 1018, containing 85% ferrite and 15% pearlite and having a hardness of 181 HB, were examined. The microstructure investigation of AISI 1018 revealed that after erosion with a particle velocity of 36 m/s and an impact angle of 30°, erosion grooves were narrower and shallower in the pearlitic region and deeper and wider in the ferrite (Fig. 13) as also pointed out by other researchers [58,75]. In the fully pearlitic AISI 1080 (Fig. 13b), damage depends on the orientation of the cementite lamellae relative to the impact direction. The pearlite plates tend to deform ahead of the abrasive particle and stack together thereby increasing resistance to further deformation. Of course, the mechanical properties of the microstructural components are important, too, as will be discussed in Section 3.4.2.

Another steel family that has recently been used in slurry transportation pipelines is the dual phase (DP) steels due to their desirable balance of hardness, strength and toughness. Dual phase steels consist of two phases – hard martensitic islands embedded in a ductile ferritic matrix [76–78]. Sharma et al. [79] compared the erosion resistance of a dual phase microstructure with the normalized, ferritic – peaerlitic microstructure of a medium-carbon steel (0.40C, 0.127Si, 0.278Mn, and 0.003Ti wt%). They concluded that the erosion resistance of a dual phase microstructure was higher than that of the normalized microstructure owing to the better coherency between the martensite and ferrite than between ferrite and pearlite. In the DP steels, the ferrite – martensite morphology and the fraction and size of the martensite islands are the crucial parameters in controlling the erosion properties [76,80]. For a given martensitic fraction, martensite islands embedded in a continuous ferritic network have been shown to exhibit better wear resistance than ferritic islands embedded in a continuous martensitic network [81,82].

Some research has been conducted to develop ferrite – bainite dual phase steels for pipeline applications [83–86]. Ji and co-workers [83] compared the standard API X70, X80, and X90 pipe steel compositions with normal and ferrite – bainite microstructures. The results showed that the fraction of high-angle grain boundaries in the dual phase microstructure was higher than the normal microstructures. These grain boundaries increase resistance to crack propagation such that the dual phase microstructure showed better toughness. In confirmation of this, Rosado et al. [84] showed that the ferrite-bainite dual phase microstructure of X120 pipe steel had the highest ultimate tensile strength amongst all the samples including lower bainite and tempered lath martensitic microstructure. They suggested that in pipelines for gas and oil transportation, where erosion is not as intensive as in slurry transportation pipelines, the optimum combinations of strength and toughness can be achieved by a ferrite-bainite dual-phase microstructure. As the predominant erosion mechanism is cutting/ploughing, it has been suggested that in the DP steel family, fine granular martensite islands provide the best microstructure for low-hardness abrasion resistant steel under mild erosion conditions, while under aggressive conditions, fine fibrous martensite improves the erosion resistance by reducing the real contact area [87].

Slurry erosion of some other ductile materials was also investigated by other researchers [88,89] including Vuorinen et al. [90], who showed that bainitic-austenitic, i.e. carbide free bainitic (CFB) microstructures, produced by austempering Si- and/or Al-rich steels have good toughness and resistance to erosion [91–94].

3.4.1.2. Brittle martensitic steels. Amongst the published studies related to the slurry erosion of steels, just a few have considered quenched martensitic steels. In 2001, Clark et al. [35] compared the erosion performance of a variety of commercial steels used in erosive slurry handling and transportation including different steel plates and steel pipes with a range of hardness values between 192 and 740 HB. The best wear performance was achieved with the hardest steel as illustrated in Fig. 14; however, the erosion mechanisms were not discussed. It has been observed that the erosion behavior can vary greatly for the materials with the same hardness level when the hardness is relatively low around 200 HV. Ojala et al. [9] reported similar results for the abrasive slurry erosion of different quenched wear resistant steels. They also revealed that the main erosion mechanism in hard materials is the formation of shear bands and their branching near the surface without any significant plastic deformation, followed by brittle cutting and micro-crack formation, as demonstrated in Fig. 15. Such a mechanism has also been observed by other researchers [72,95]. For example, Sooraj and Radhakrishnan [96] have shown that when a particle strikes a brittle surface, it creates sidelong and radial micro-cracks, which start to grow and propagate during the following impacts. These cracks cause the surface to split into smaller pieces, which can be removed by the subsequent impacts.

Also, in the case of H13 tool steel with a hardness of 595 HV, Rodriguez et al. [97] showed that, under high strain rate and normal impact, adiabatic shear bands (ASB) are the preferred path for the

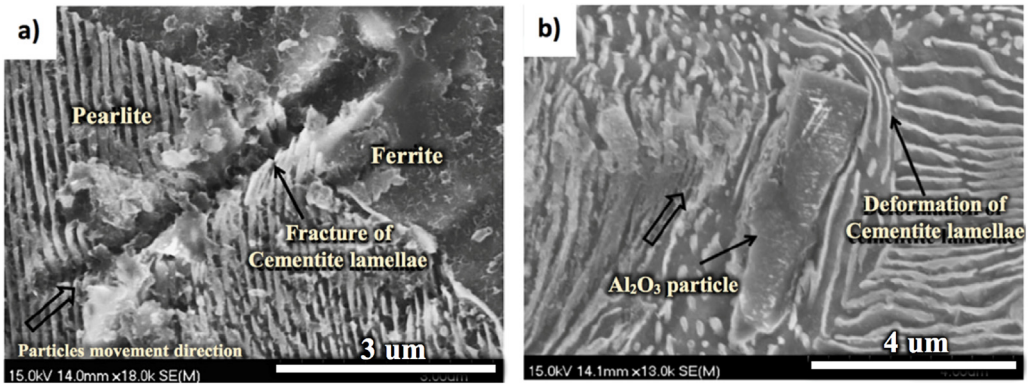

Fig. 13. a) Erosive particle impacts on pearlite and slides towards ferrite in AISI 1018. b) Erosive particle impacting parallel to the cementite lamellae in AISI 1080 [74]. (SEM micrographs of samples after a sand blast type erosion test using aluminum oxide particles at an impact angle of 30°).

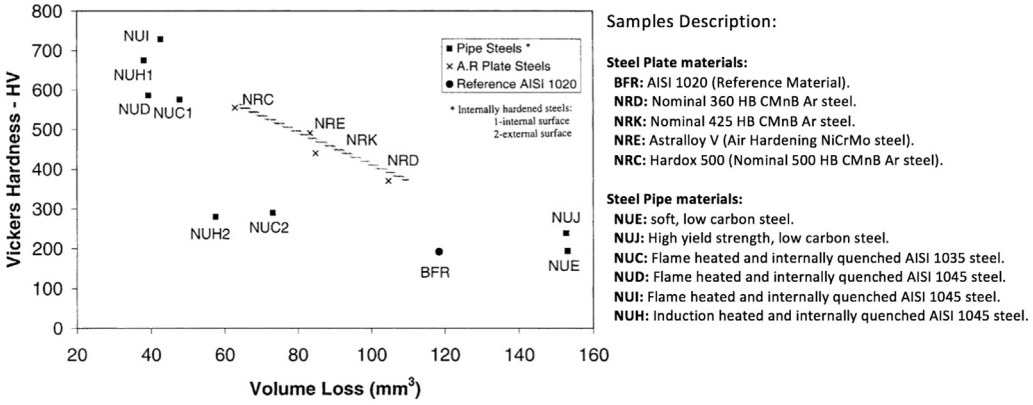

Fig. 14. Volume loss and average near-surface hardness data for steel plate and steel pipe materials [35].

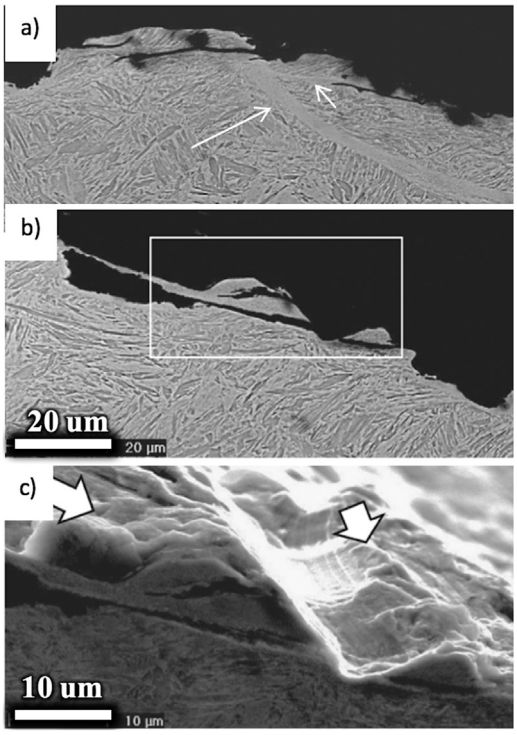

Fig. 15. SEM images of a steel with a hardness of 500HB after a high-speed slurry pot test with a slurry containing 33 wt% granite particles 8–10 mm in diameter. Sample angle 45°. a) Cross-section showing lack of significant surface deformation and a branched shear band. b) Cross-section showing eroded surface and crack formation. c) A 3D image at higher magnification showing the deformed and eroded surface layer. Steel composition in wt% 0.3C, 0.8Si, 1.7Mn, 1Cr,1Ni, and 0.5Mo. [9].

propagation of the subsurface cracks, thus promoting greater erosion damage, see Fig. 16.

Haiko et al. [95] also revealed that under high-load impingement of large particles (10–12.5 mm) on brittle steels, apart from shear band formation, orientation and fibering of the martensite laths in the deformed layer near the target surface also occurred, see Fig. 17.

Looking into these mechanisms in more detail, Mukhopadhyay et al. [98] have done an advanced microstructural evaluation of a quenched and tempered AISI 52100 steel (1.00C, 0.30Mn, 0.36Si, and 1.46Cr wt% during normal and oblique erosion. They reported that the fraction of low-angle grain boundaries was larger after oblique erosion while fewer shear bands were produced after oblique erosion compared to normal erosion (Fig. 18). In other words, normal erosion results in a higher strain rate which leads to the formation of shear bands and reduced strain localization. TEM bright field examination also revealed that normal and oblique erosion caused martensite lath boundaries to disintegrate and recovered islands to form.

3.4.2. Mechanical properties

The use of mechanical properties to estimate the erosion rate of materials has been always an attractive subject thanks to the low cost, simplicity and availability of data for many materials. As mentioned before, it is generally believed that material hardness is one of the most important parameters affecting the erosion behavior of a wide range of materials [21,50,51,99–102]. Accordingly, Oka et al. [103,104] reported that material hardness followed by the particle properties and impact velocity are the predominant parameters governing erosion damage. They proposed the following relationship for the total erosion (E_T):

$$E_T = KV_P^m d_P^n H_T^{K_1} \sin\alpha^{n_1} (1+H_T(1-\sin\alpha))^{n_2} \quad (14)$$

where V_P is the impact velocity (ms^{-1}), d_P is the particle diameter (μm), H_T is the material hardness (GPa), m, n and K_1 are experimentally determined exponents, and K, n_1 and n_2 are constants that depend on material properties of the particles and target.

Despite the fact that increasing hardness is generally believed to reduce erosion, some researchers believe that the material hardness is not necessarily a good indicator for predicting the erosion rate, and that other mechanical properties should also be considered [51,105,106]. For instance, O'Flynn et al. [102] evaluated the erosion rate of two heat treated steels, a eutectoid 0.8% C steel (EN42) and a 0.4% C low alloy steel (EN24) with 12 different microstructures and hardness values. Studying three different particle impact angles (8, 30 and 90°) and a particle velocity of 15 m/s, they revealed that the erosion resistance of a pearlitic microstructure with a hardness of 25 HRC was better than that

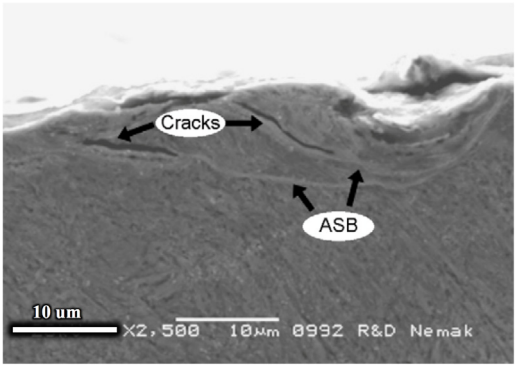

Fig. 16. Cross-section of an eroded specimen with hardness 595 HV showing adiabatic shear bands (Test rig: a sand blasting type machine and impact angle 90°) [97].

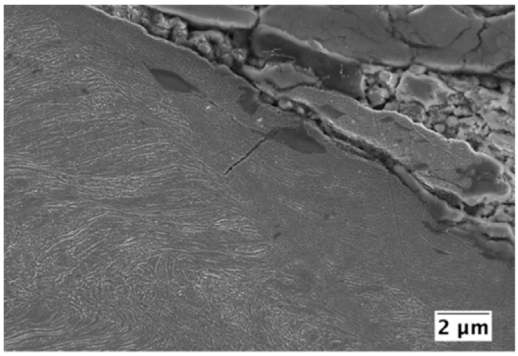

Fig. 17. Fibering in a martensitic microstructure containing 0.35 wt% carbon after a heavy impact erosion test with 10–12 mm diameter granite gravel particles [95].

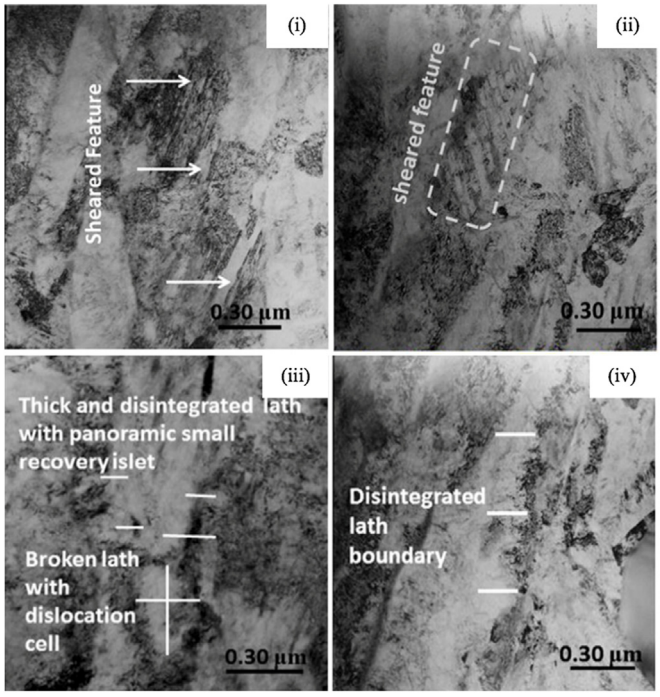

Fig. 18. Micrographs of 52100 steel. Sheared features of tempered martensite laths after (i) oblique incidence (impact angle 30°) and (ii) normal incidence. Thick and disintegrated lath boundary with small recovery islet after (iii) oblique (particle impact angle of 30°)and (iv) normal erosion [98]. (Erosion test: A jet erosion type tester with silica particles and impact velocity of 105 m/s).

of a 35 HRC bainitic microstructure, and even better than that of martensitic microstructures with hardness as high as 55 HRC. The erosion rate of these specimens is presented in Fig. 19. Similar results were also reported for particle velocities of 25 m/s and 35 m/s. This result was in agreement with Levy's work [21] which showed that, owing to differences in the distribution of fine carbides, a spheroidized AISI 1075 steel with a hardness of 79 HRB was more resistant to erosion than both fine and coarse pearlitic microstructures with hardness values of 100 and 90 HRB, respectively.

Based on the assumption that, due to the high strains and strain rates involved, particle impacts result in local heating, O'Flynn et al. [102], proposed that erosion resistance can be related to the product of tensile toughness and uniform elongation strain. Tensile toughness is the energy required to produce fracture as given by the area under the true stress - true strain curve in a tensile test. It was demonstrated that the total erosion rate increases as the product toughness × uniform strain decreases.

According to Ukpai et al. [107], the fracture or deformation energy of erosion can be measured experimentally using a wideband piezoelectric sensors to detect and measure the acoustic emission waves resulting from the erosion. Hutchings [108] demonstrated that this transient elastic energy can be between one and five percent of the kinetic impact energy of the particles.

Since material removal is mostly related to the formation and growth of lateral cracks, some empirical and theoretical models of erosion rate are based on the mechanical properties of the target, i.e. hardness and fracture toughness. Examples of these are the models of Evans et al. [109] for brittle ceramic materials, Hutchings [110] for ductile materials like aluminum alloys, Johansson et al. [111] for brittle single crystals of silicon and Levin et al. [112] for various metallic alloys. However, the details of these are not covered in this review as they are not related to the slurry erosion of steel.

4. Test methods and models for evaluation of slurry erosion

Slurry erosion test methods can basically be categorized into two main groups: pilot pipeline erosion tests and laboratory simulation tests [113]. Laboratory test equipment generally accelerates erosion by increasing loads, velocities or other operational parameters. Furthermore, laboratory testing is widely used owing to its low cost, easy set up and operation, and short test duration, although pilot-scale testing can generate conditions closer to industrial practice. The laboratory test equipment, also commonly known as bench scale test rigs, are the most popular method to study the effect of various parameters on erosion and to better understand erosion mechanisms. Hence, many investigations have been carried out to design or improve test rigs in order to evaluate the slurry erosion behavior of different materials under different conditions and to eventually develop general models. As each test rig and proposed model was the result of a very specific approach, no test rig is yet available that can fully simulate real practical erosion conditions and also no universally accepted model exists. Therefore, attempts to scale up or extrapolate specific test rig data or model predictions can lead to significant errors. Moreover, almost all models rely to some extent on the experimental determination of empirical coefficients. Therefore, in this review, each test rig method and the models based on that specific test rig are discussed individually in order to better understand the differences between them.

The slurry pot tester and slurry jet tester have become the two most popular test arrangements, being used in almost 50% of recently published research. However, we also review the procedures of some the other frequently used test methods in this section too. For information about the following, less common, bench scale test rigs the reader is referred to the original publications: gas gun [114], contra-rotating disc tester [115], sliding bed erosion test fixture [116], flow-through slurry wear tester [117], submerged impinging jet [118], sand-hydroblast [119], high-temperature erosion test [120], Miller tester [121] and pin abrasion test [122].

It should be also noted that erosion data is reported differently by different investigators, e.g., erosion is given in terms of mass, volume or thickness loss. Therefore, in order to compare erosion rates from different test rigs and using different flow conditions, the erosion rate should be normalized for example with respect to the slurry flow rate [22]. To obtain a normalized erosion rate, the mass erosion rate (mg/s) should be divided by the slurry mass flow rate (mg/s), where the erosion rate of the specimens is calculated from the slope of the mass loss vs time plots and the slurry flow rate is calculated by measuring the total slurry mass flow, i.e. that of the liquid and abrasive particles, per unit time.

$$Normalized\ erosion\ rate = \frac{Erosion\ rate \quad (\mathrm{mg\ s^{-1}})}{Slurry\ flow\ rate \quad (\mathrm{mg\ s^{-1}})} \tag{15}$$

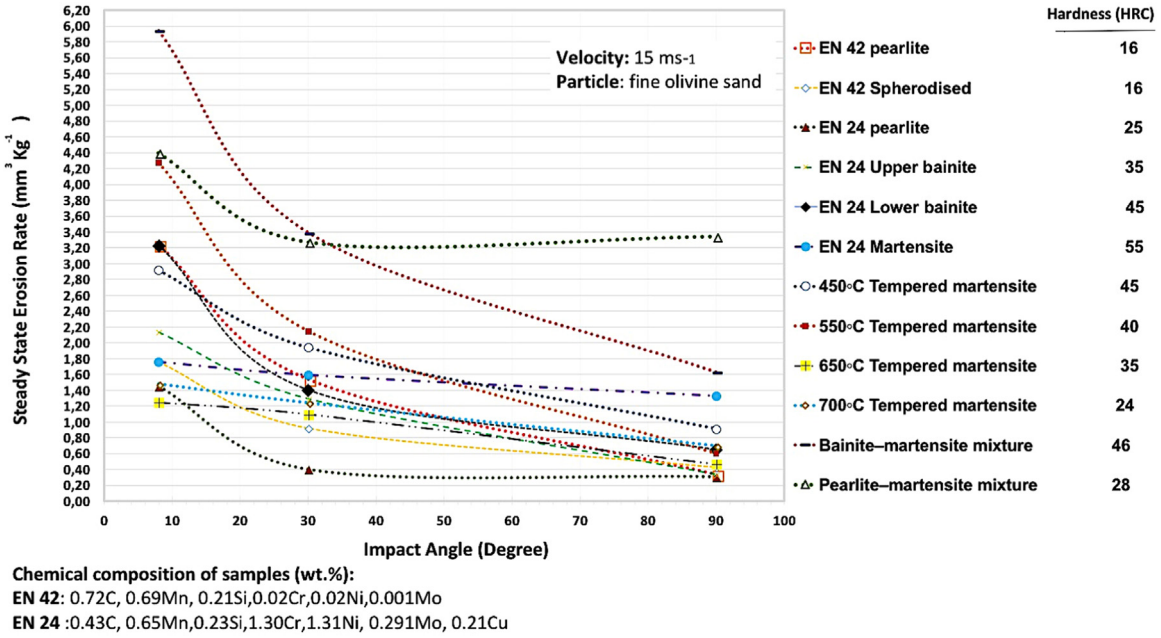

Fig. 19. Effect of hardness and microstructure on steady state erosion rate. Data source: O'Flynn et al. [102].

4.1. Pot tester

The first slurry pot tester was designed and fabricated by Gupta et al. [46] in 1992, and it is still the most popular test rig. This machine consists of a cylindrical chamber, shaft, stirrer arrangement, set of bearings, motor, and rotating arms as the main components, see Fig. 20. A mixer propeller is attached to the bottom of a steel shaft, which is rotated inside a cylindrical tank to keep the particles in the slurry in a suspended state in the aluminum [46] or stainless steel [123] chamber. Slightly above the propeller, a brass sleeve is provided for fitting four flat side arms holding the erosion test samples. U-shaped baffles on the cylindrical tank walls also help keep the particles in a suspended state and break up the rotational motion created by the propeller. The shaft can be rotated at different speeds by a variable speed motor [46]. In this test method, the rotating slurry velocity, particle impact angle and slurry concentration can be controlled. However, because of significant differences in the nature of the hydrodynamic flow conditions compared to actual pipe flow, the results need to be interpreted with caution if they are used to predict slurry erosion in real pipe systems.

According to Desale et al. [124], the main concerns about this test are related to the homogeneity of the slurry and turbulence inside the pot, which limit the validity of the data generated in respect of quantitative analysis. Therefore, to improve the distribution of solids at lower speeds and minimize the effect of propeller rotation, they tried to improve the pot section by assisting four-bladed propellers pitched at 45° operating in a down-pumping mode instead of the marine or butterfly type propeller, see Fig. 21. The improvements also included a transparent tank to allow the solid–liquid suspension characteristics to be studied, and a slotted angular plate (Fig. 21b) to orient the test fixtures at any angle in the range of 0–90° in steps of 15°.

In 2010, Gadhikar et al. [125] developed an improved design of pot erosion tester that could handle both large cylindrical and flat samples and also allow slurry characteristics to be varied, i.e., slurry volume as well as erodent particle concentration and size. For this purpose, they used separate DC motors for rotating the stirrer and the sample holder. For checking the actual solid concentration at different heights from the bottom, the tank was provided with four outlets at different heights along the wall (T_1-T_4). A schematic illustration of the experimental set up and details of the modified slurry erosion pot tester is given in Fig. 22.

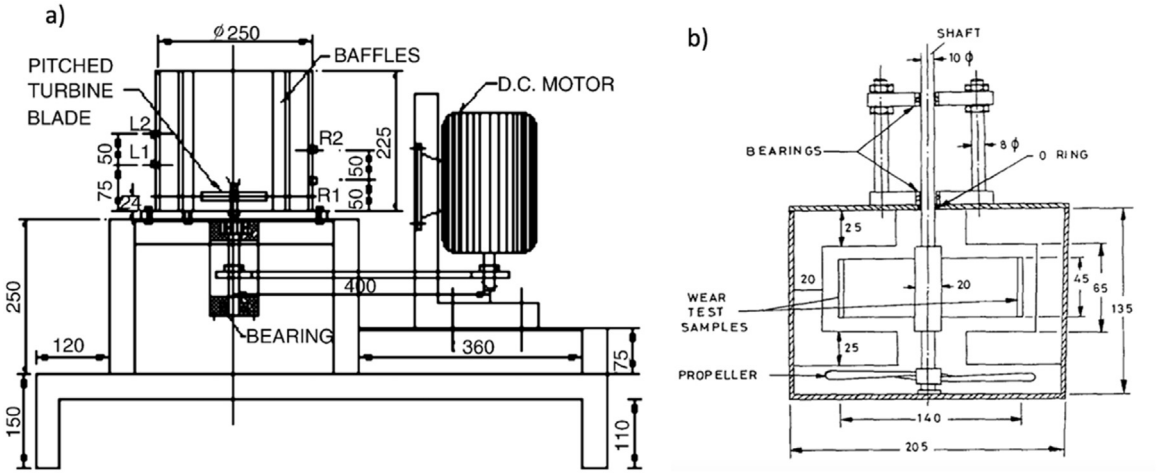

Fig. 20. a) Schematic illustration of a typical slurry pot tester machine [124], b) details of pot section [46].

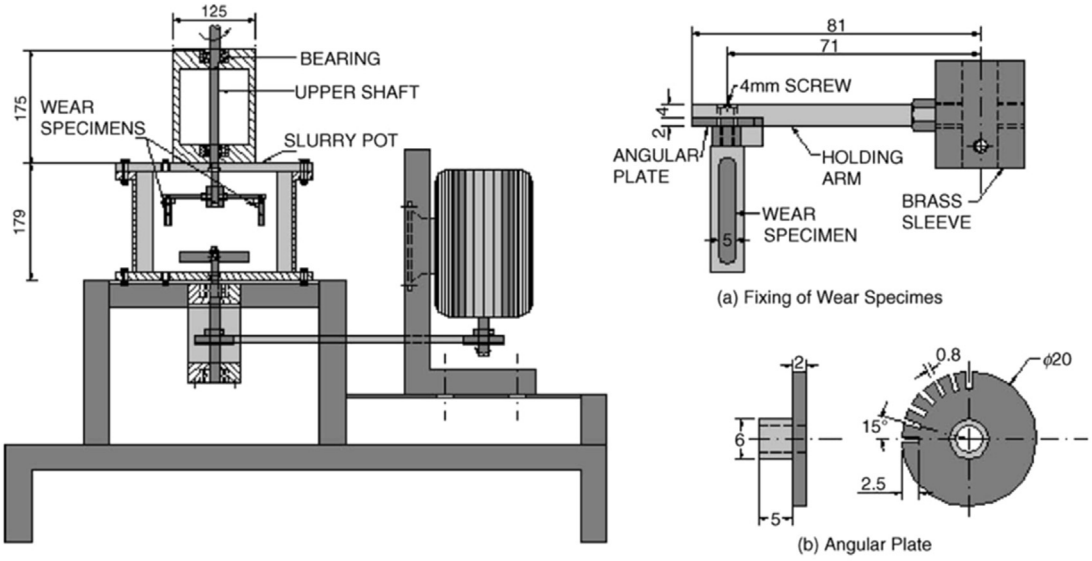

Fig. 21. Schematic illustration of improved pot tester: (a) fixing of wear specimens; (b) angular plate [124].

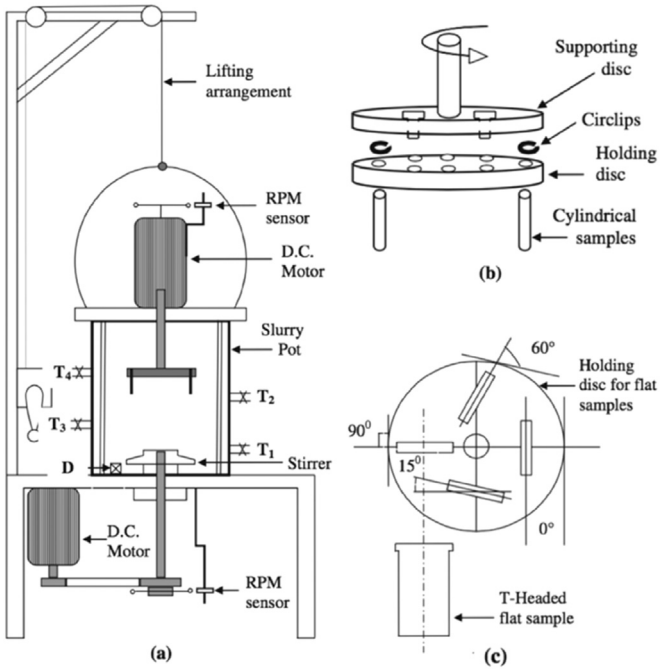

Fig. 22. a) Schematic illustration of the modified slurry pot erosion tester set up. b) Specimen holder details for circular samples. c) Holding disc with different orientation angles for flat samples [126].

In 2015, Tampere Wear Center [73,90] designed a high-speed slurry-pot tester to simulate erosion in industrial slurry pumping. This modification provided a possibility to evaluate the erosion of different types of large samples under harsh erosive conditions using large particle sizes. The sample types were round samples with a diameter of 18.5–26 mm, square samples with a cross-section of 15 × 15 mm, and plate samples with dimensions 64 × 40 × 6 mm. Moreover, speed levels up to 20 m/s at the specimen tip can be reached with large abrasive sizes up to 10 mm. Fig. 23 presents schematic and photographic views of a pin mill type of slurry-pot tester with round samples [126].

In order to predict the erosion rate using the slurry pot test, Gupta et al. [46] proposed a power law relationship on the basis of the investigations of Elkholy [127] giving:

$$E_T = KV_P^{\,m} d_P^{\,n} C_W^{\,p} \tag{16}$$

where E_T is the total erosion rate; V_P, the solid particle velocity; d_P, the diameter the solid particles, C_W, the concentration of solid particles in the slurry, and k, m, n and p are constants which are dependent on the target material and slurry properties. Gupta et al. [46] empirically determined the constants for brass and mild steel. Other researchers [47,89,128] subsequently evaluated the constants for other materials. Later [129], Eq. (16) was extended to take into account the impact angle and particle density:

$$E_T = KV_P^{\,m} d_P^{\,n} C_W^{\,p} \alpha^q \rho_P^{\,r} \tag{17}$$

The problem with the above empirical equations is that the values of the constants vary over a wide range depending on the materials and test conditions. This can be seen from the examples of the reported values for the power indices for different materials listed in Table 2.

Hence, many attempts have been made to develop a more general relationship by including other parameters [34,89,131]. For example, material properties like toughness of target material or particle hardness are taken to the consideration by Wiederhorn and Hockey [131]. They proposed that erosion rate can be expressed as:

$$E_T = KV_P^{2.8} r_P^{3.9} \rho_P^{1.4} k_T^{-1.9} H_P^{0.48} \tag{18}$$

where r_P, ρ_P, k_T and H_P are the particle radius, particle density, target material fracture toughness and particle hardness, respectively.

Later, Desale et al. [34,128,132] investigated the effect of target hardness by performing a large number of slurry pot tests on a wide range of ductile materials, e.g. mild and stainless steel, copper, aluminum. They developed an empirical model based on the assumption that total erosion rate (E_T) in ductile materials is the sum of the contributions from deformation (E_D) and cutting (E_C) erosion rates; i.e. $E_T = E_D + E_C$. They proposed that the erosion rate under normal impact conditions is given by:

$$E_{90} = 6.62 \times 10^{-14} K_{(H_P/H_T)} V_P^{2.02} d_P^{1.62} C_W^{-0.285} \tag{19}$$

where $K_{(H_P/H_T)}$ is a constant as function of the ratio of particle hardness (H_P) to target material hardness (H_T) which is defined as:

$$K_{(H_P/H_T)} = 0.42, \quad \text{if} H_P/H_T \leq 6$$

$$K_{(H_P/H_T)} = 1.00, \quad \text{if} 6 \leq H_P/H_T \leq 12.30$$

$$K_{(H_P/H_T)} = 1.83, \quad \text{if} 12.30 \leq H_P/H_T$$

The deformation erosion contribution for non-normal impact was given as [132]:

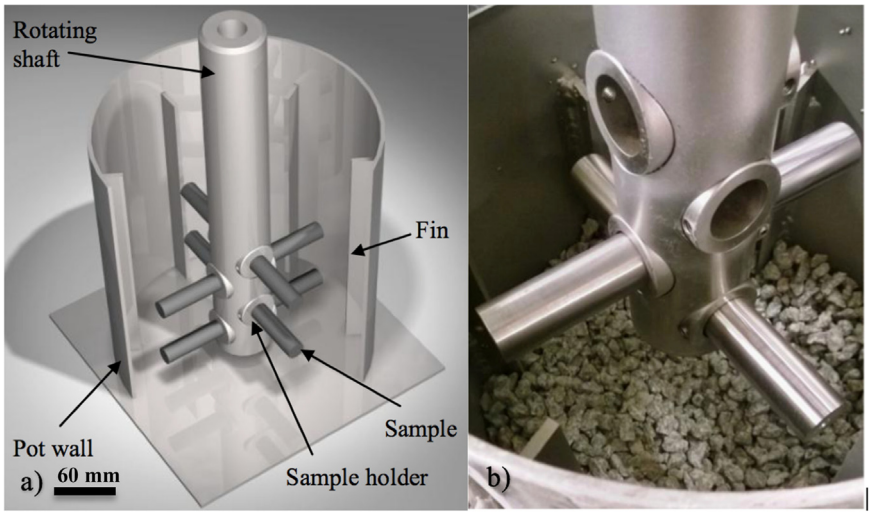

Fig. 23. a) Schematic illustration of high speed pot tester [127]. b) Photographic view of the same [92].

Table 2
Some of the reported power index constants in Eq. (17) for different materials.

Ref.	Material	K	m	n	p	q	r
Gupta [46]	Mild Steel	0.223	2.148	0.344	0.556	–	–
Gupta [46]	Brass	0.178	2.488	0.291	0.516	–	–
Gandhi [47]	Brass	2.570	2.560	0.850	0.830	–	–
Patil [89]	Aluminum	0.075	3.350	1.370	1.090	0.120	–
Huang [130]	SAE-1055 Steel	0.082	2.375	0.500	–	*	0.187
Desale [128]	Ductile Material#	Eq. (21)	2.350	1.550	−0.110	Eq. (25)	–

* α^{q} is replaced by: $(\cos\alpha)^2(\sin\alpha)^{0.375}$.
\# E.g. mild steel, AISI 316L, Copper, Brass.

$$E_D = E_{90}(\sin\alpha)^3 \tag{20}$$

Similarly, the final relation obtained for the cutting erosion contribution was:

$$E_C = 6.204\times10^{-12} f(\alpha)(MS_F)^{-0.80} H_T^{-0.72} V_P^{2.35} d_P^{1.55} C_W^{-0.11} \tag{21}$$

where MS_F is a modified shape factor,

$$f(\alpha) = \begin{cases} 0.99\left[\sin\left(\frac{\pi}{2}\right)\left(\frac{\alpha}{\alpha_{Max}}\right)\right]^{0.58} & for\ \ 0^\circ \le \alpha \le \alpha_{Max} \\ 0.92\ \left\{\left[\sin\left(\frac{\pi}{2}\right) - \left(\frac{\pi}{2}\right)\left(\frac{\alpha-\alpha_{Max}}{90-\alpha_{Max}}\right)\right]\right\}^{4.30} & for\ \ \alpha_{Max} \le \alpha \le 90^\circ \end{cases} \tag{22}$$

and

$$\alpha_{Max} = 0.55 H_T^{0.69} \tag{23}$$

4.2. Jet erosion tester

The slurry jet erosion tester is the second most commonly used erosion test rig which is also commonly used to develop both empirical and CFD erosion models as it facilitates the easy control test parameters like particle velocity and impact angle. In this test bench procedure, the specimen is continuously eroded by the impact of fresh slurry flow [50]. It comprises a slurry/particle reservoir, a slurry pump, or in a dry test a compressor, a specimen holder, a nozzle and controlling valves and equipment. The wet type is illustrated in Fig. 24 [129]. The specimen holder can be adjusted to provide different slurry impingement angles. In the dry type, erosion is simulated by feeding the solid particles at a constant rate from the main reservoir into the pressurized particle tank, where a mixture of solid particles and air is created and then accelerated by a compressor thereby forcing the mixture through a converging nozzle [97]. In order to directly measure the particle velocity without disturbing the particle flow, Lindsley and Marder [72] used a TSI Laser Doppler Velocimeter (LDV) instead of an ordinary manometer or flow meter. The jet erosion test is not recommended for simulating slurry erosion in pipelines as the velocity is much greater than would ever be observed in an operating slurry pipeline, but it is really one of the best for ranking different materials.

One of the earliest semi-empirical equations to predict erosion rate in jet erosion testing was proposed by Tabakoff et al. [133]. They consider the effect of particle tangential restitution ratio (P_{TR}) as defined below and derive the following equation, which characterizes the erosion rate under small and large impingement angles:

$$E_T = K_1 V_P^2(\cos^2\alpha)(1-P_{TR}^2) f(\alpha) + K_2[V_P\sin\alpha]^4 \tag{24}$$

where

$$f(\alpha) = \left\{1+K_3\left[K_4\sin\left(\frac{\pi}{2}\frac{\alpha}{\alpha_{Max}}\right)\right]\right\}^2 \tag{25}$$

$$P_{TR} = 1 - 0.0016 V_P\sin\alpha \tag{26}$$

$K_3 = \begin{cases} 1, & \alpha \le 3\alpha_m \\ 0, & \alpha > 3\alpha_m \end{cases}$ and α_m is the angle of maximum erosion, K_1, K_2, and K_4 are empirical constants which depend on the particle and material properties. The uniqueness of this relationship was the major

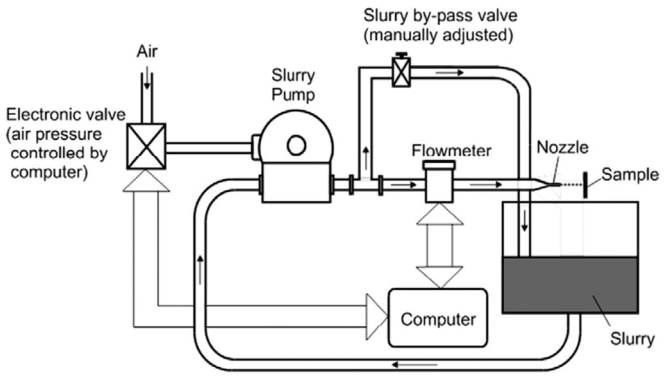

Fig. 24. Schematic showing a jet erosion test setup for wet slurry [129].

role of the particle tangential restitution. Menguturk and Sverdrup [134] also developed an empirical erosion model for carbon steel under jet erosion based on the same parameters, but excluding the restitution. The volumetric erosion rate ($mm^3\ g^{-1}$) for a wide range of impact angles is given as:

$$E_T = \begin{cases} 1.63 \times 10^{-3}(V_P\cos\alpha)^{2.5}\sin\left(\frac{180}{45.4}\alpha\right)+4.68\times10^{-7}(V_P\sin\alpha)^{2.5} & \alpha \le 22.7^\circ \\ 1.63 \times 10^{-3}(V_P\cos\alpha)^{2.5}+4.68\times10^{-7}(V_P\sin\alpha)^{2.5} & \alpha > 22.7^\circ \end{cases} \quad (27)$$

By running different jet erosion tester conditions Elkholy [127] proposed an analytical model for predicting the erosion of brittle, hard materials. By assuming that the impact angle is independent of particle velocity, the erosion rate, expressed as the mass of material (g) removed in unit time (min), was predicted to follow the equation:

$$E_T = KC_W^{0.682}\left(\frac{H_T}{H_P}\right)^{k_1} d_P^{0.616}V_P^{2.39}\left\{1+\sin\left(\frac{180(\alpha-\alpha_1)}{90-\alpha_1}-90\right)\right\} \quad (28)$$

where K is an empirical material dependent constant (1.342×10^{-5} for cast iron), C_W is the slurry concentration by volume, H_T and H_P are the Brinell hardness (HB) of target material and particle; α, d_P, and V_P are the particle impact angle (°), size (mm) and velocity (m/s), respectively. α_1 is the angle at which erosion starts during the experiments and for the simplicity can be taken as zero. The value of k_1 was reported as 3.817 when $\frac{H_T}{H_P}<1.9$ and 0.268 if $\frac{H_T}{H_P}>1.9$

Ahlert [135] conducted a series of jet erosion type tests on a cold rolled AISI 1018 steel using different particle shapes. He stated that the total erosion rate by the solid particles depends on the target material hardness, particle shape factor, impact angle and velocity. An empirical power-law relationship was proposed:

$$E_T = KH_T^{-0.59}S_F V_P^m f(\alpha) \quad (29)$$

where K is an empirical constant, H_T is the material hardness on the Brinell scale, S_F is a particle shape factor empirically proposed to be unity for sharp (angular) particles, 0.53 for semi-rounded particles, and 0.20 for fully rounded particles. The value of m was reported as 2.41 by Ahlert [135] and, later, considered equal to 1.73 by Wang and Shirazi [136]. f(α) is a function of particle impact angle, which according to Wang and Shirazi [136] can be defined as:

$$f(\alpha) = \begin{cases} K_1\alpha^2 + K_2\alpha & 0 \le \alpha < 15^\circ \\ K_3\cos^2\alpha\sin\alpha + K_4\sin^2\alpha + K_5 & 15^\circ < \alpha \le 90^\circ \end{cases} \quad (30)$$

and according to Zhang et al. [137] defined as:

$$f(\alpha) = \sum_{i=1}^{5} A_i\alpha^i \quad (31)$$

In Eq. (31), the value of the constants K_i for i = 1–5 and A_i were determined empirically. Zhang et al. [138] gave $K = 2.17\times10^{-7}$ and m = 2.41 for the carbon steel with spherical particles, while Wang et al. [136] gave $K = 1.95\times10^{-5}$ and m = 1.73 for the carbon steel with semi-rounded particles for both dry and wet slurry conditions. Recently, Karimi et al. [139] showed that the model works better for the wet slurry compared to the dry slurry.

Haugen et al. [140] examined 28 different materials taking into account the mass of the impacting particles (M_P), particle velocity and impact angle under jet erosion conditions. They developed the following relationship for the total erosion rate:

$$E_T = KM_P V_P^m f(\alpha) \quad (32)$$

The function f(α) for carbon steel was given as:

$$f(\alpha) = \sum_{i=1}^{8} -1^{(i+1)}A_i\left(\frac{\alpha\pi}{180}\right)^i \quad (33)$$

It has been pointed out that the model coefficients K and m are strongly dependent on the material type.

Oka et al. [103,106] also proposed a similar empirical relationship taking into account the effect of target material properties (e.g. hardness, work hardening) and particle properties (e.g. particle diameter and velocity). The final modified version of their relationship is given in Eq. (34).

$$E_T = K(K_4H_T)^{bK_1}\left(\frac{V_P}{v'}\right)^m\left(\frac{d_P}{d'}\right)^n f(\alpha) \quad (34)$$

where H_T is the target material hardness (GPa); V_P and d_P are the particle velocity ($m\,s^{-1}$) and diameter (μm), respectively. K, K_1 and n

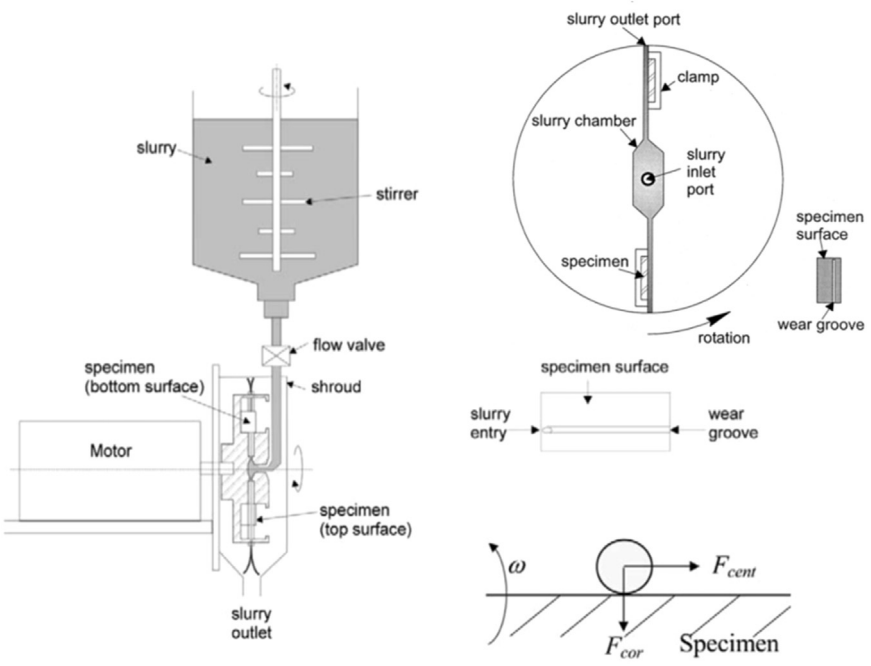

Fig. 25. Schematic diagrams of the modified (Mark II) Coriolis slurry erosion tester with experimental setup details [2,80].

exponents which can be empirically determined from the particle properties, and m is a function of particle properties and material hardness. v′ and d′ are experimentally determined standard impact velocity and standard particle diameter. f(α) is a function of impact angle given by $\sin\alpha^{n_1}(1+H_T(1-\sin\alpha))^{n_2}$.

Huang et al. [130] developed the following mechanistic model for erosion under jet flow conditions. Like the other mechanistic models, it has been proposed that the total erosion magnitude is the sum of cutting and deformation damage. In the case of cutting damage, the material removal shows a power-law relationship to particle size, mass, impact velocity and angle in which the exponents are mainly determined by the particle shape. In the case of deformation damage, all the exponents, except the particle mass, are dependent on the properties of the target material. The work hardening characteristics and ductility of the target material were considered as crucial material properties.

$$E_T = C\frac{M_P{\rho_P}^{1/4B}(V_P\sin\alpha)^{2+1/2B}}{{\varepsilon_{cr}}^{1/B}{P_n}^{1+1/4B}} + D\frac{{M_P}^{1+3(1-n)/4}{V_P}^{2+3(1-n)/2}(\cos\alpha)^2(\sin\alpha)^{3(1-n)/2}}{{d_P}^{(1-n)/4}{\varepsilon_0}^i{P_t}{P_n}^{3(1-n)/4}} \quad (35)$$

M_P, ρ_P, V_P, d_P and α are the particle mass, density, velocity, size, and impact angle, respectively. P_n is a function of the material work hardening behavior and P_t represents the material plastic flow stress (N/mm^2); ε_{cr} is the critical strain and ε_0 is a function of the target material ductility. C and D are equation coefficients, and B and i material dependent exponents, that need to be determined experimentally; n is a constant which depends on the particle shape taking a value between 0.5 for sharp particles and 1.0 for round particles.

Later, using Eq. (35) in conjunction with a CFD model, a new equation has been developed by Wang et al. [65]:

$$E_T = K_1\frac{{M_P}^{1.125}{V_P}^{2.25}(\cos\alpha)^2(\sin\alpha)^{0.25}}{(1+B)^{0.25}{S_T}^{0.125}{H_T}^{0.7}{e_T}^{1.2}} + K_2\frac{{S_T}^{1.1}{d_P}^{0.05}}{{H_T}^{0.98}{e_T}^{1.44}}\left(\frac{(M_P{V_P}^2\sin^2\alpha)}{1+B}\right)^{1.15} \quad (36)$$

where K_1 and K_2 are empirically determined material constants. In the case of the Canadian 44W carbon structural steel (0.26%C, Max. 0.40% Si, max. 0.90%Mn, equivalent to ASTM A36, for example) $K_1 = 7.48\times10^{-4}$ and $K_2 = 0.283\times10^{-6}$. S_T, H_T, and e_T are the stiffness, hardness and elongation of target material, respectively. B is defined as the ratio of target material stiffness to the particle strength. M_P, V_P, d_P and α have the same meanings as in Eq. (35).

4.3. Coriolis erosion tester

Tuzson et al. [35,116] developed the Coriolis erosion test to simulate the erosion conditions which are experienced in rotary slurry systems such as pumps and cyclones. This instrument consists of two principal parts, a steel rotor and a diametrical channel with two flat specimens equidistant from the center. At high rotation speeds, slurry flows outwards from the center by a centrifugal force and the Coriolis force increases the slurry interaction with the back wall of the samples [141]. Clark and co-workers [142] developed an improved version, which is schematically illustrated in Fig. 25. It should be noted that this design is completely different from the type used by Walker and Hambe [28] which consisted of a rotating distributor system containing a bowl and four slurry channels. In the modified version, each specimen holder contains a channel with a rectangular cross-section, the bottom of which is formed by the test specimens (Fig. 25 top right). Fresh slurry is supplied to a central chamber and forced outwards by an electric motor driven rotor turning at speeds up to 7000 rpm. As a result of the accelerated slurry flow, the solid particles in the slurry are forced to settle out and bear down on the test samples. Slurry is supplied by gravity from a mixing tank above the rotor and the particles are kept in suspension by using a rapidly rotating impeller. Slurry is delivered through a circular orifice to control the rate of the slurry flow [142]. Recently, to provide better control of the slurry flow over the test specimen surface, Hawthorne et al. [143] developed a new design of the rotor – specimen holder assembly to remove the small step in the channel between the holder and the specimen surface by using longer specimens, as illustrated in Fig. 26. It has to be noted that in comparison with the slurry pot test method and real industrial pipelines conditions, particle and slurry velocities are typically much higher here. However, the test duration is very short, which makes the Coriolis erosion tester the most suitable test rig for the ranking of the erosion resistance of wide ranges of materials, including hard and ductile materials.

Tuzson [35,116] proposed that the local erosion rate under the Coriolis condition is the ratio of the friction power per unit area (P_F) in J/m^2 to the specific energy (E_S) in J/m^3, i.e.:

$$E_T = P_F/E_S \quad (37)$$

E_S is determined experimentally based on the erosion depth and time:

$$E_S = (\rho_P - \rho_L)\omega^2 R_{Ch} C_0 (Q/W)(t/h) \quad (38)$$

Here, ρ_P and ρ_L are the densities of the solid particles and the carrier liquid, respectively, ω is the rotational (angular) rotor velocity, R_{Ch} is the mean Coriolis channel radius (from the axis of rotation), C_0 is the

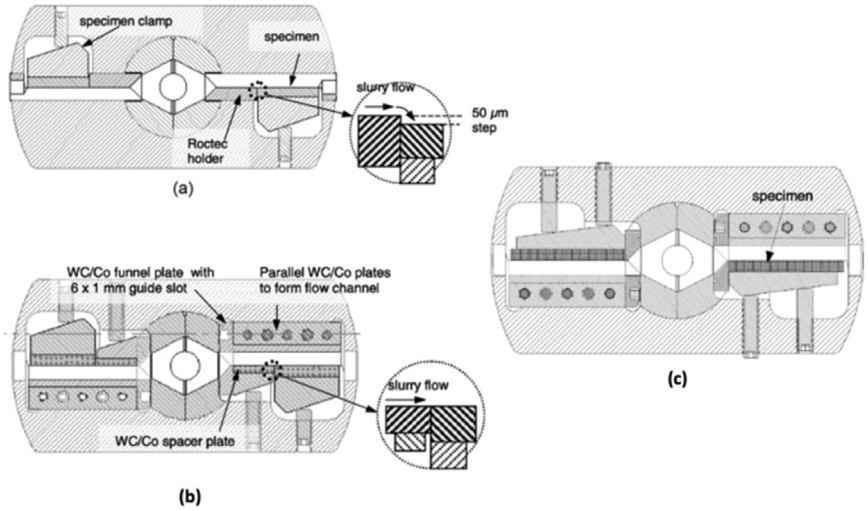

Fig. 26. (a) The step details between the holder and the sample surface. (b) Initial modification. (c) Final modified specimen holder [143].

volume of delivered slurry, Q is the volumetric flow rate, and W is the passage width. t and h are the erosion time and erosion depth, respectively.

According to Tian et al. [144], P_F can be calculated as:

$$P_F = \tau u_P \tag{39}$$

where τ is the shear stress between the eroded surface and the particulate phase and u_P is the tangential velocity of the solid particles.

Assuming that a suspended particle is subjected to a centrifugal force ($F_{cent.}$) and a drag force (F_{dr}), Xie et al. [145] showed that the radial particle velocity ($\frac{dr_p}{dt}$) is given by the following non-linear differential equation.

$$M_P \frac{d^2 r_p}{dt^2} = F_{cent.} - F_{dr} = M_P \omega^2 r_p - \frac{1}{2} C_{dr} \rho_L A_P \left(\frac{dr_p}{dt} - \frac{dr}{dt} \right)^2 \tag{40}$$

where M_P is the particle mass, ρ_L is the carrier liquid density; C_{dr} is the drag coefficient between the particle and surrounding slurry; A_P is the projected area of the particle and $\frac{dr}{dt}$ is the velocity of the surrounding slurry. r is the instantaneous location of liquid unit and r_p is the instantaneous location of the particle during the radial movement.

For the particle velocity normal to the target surface ($\frac{dy}{dt}$) the following equation applies.

$$M_P \frac{d^2 y}{dt^2} = F_{cent.} - F_{dr} = 2 M_P \omega^2 \frac{dr_p}{dt} - \frac{1}{2} C_{dr} \rho_L A_P \left(\frac{dy}{dt} \right)^2 \tag{41}$$

Pagalthivarthi et al. [146–149] proposed a model to predict the erosion rate caused by a multi-sized particulate size slurry in Coriolis testing. Their approach is based on the total erosion rate being the sum of *impact erosive wear* (W_I) and *sliding erosive wear* (W_s):

$$E_T = W_I + W_s \tag{42}$$

By extending the model for mono-sized slurries proposed by Roco et el. [150], they showed that *impact wear* for the multi-sized particulate slurry can be calculated as:

$$W_I = \sum_{k=1}^{N} \frac{\rho_{P,k} C_{w,k} {V_{P,k}}^3}{f(\alpha_k, d_{p,k})} \tag{43}$$

where $\rho_{P,k}$, $C_{w,k}$, and $V_{P,k}$ are the density, slurry concentration and velocity of the specific particle class size k and $f(\alpha_k, d_{P,k})$ is a specific energy coefficient, a function of particle impact angle and particle diameter in each size class, which needs to be determined empirically. Note that $\rho_{P,k} C_{w,k} V_{P,k}$ is the mass flux and ${V_{P,k}}^2$ is the kinetic energy per unit mass of the particles for the k^{th} species.

They also proposed that the *sliding wear* rate can be expressed as the ratio of friction power (associated with shear stress and particle tangential velocity) to the specific energy of sliding, giving:

$$W_S = \sum_{k=1}^{N} \frac{C_{w,k} u_{P,k} \tau_k}{E_{S,k}} \tag{44}$$

where $u_{P,k}$, τ_k are the shear stress and tangential velocity of the particulate species k; and $E_{S,k}$ is the particle size dependent specific energy for sliding, which is defined as:

$$E_{S,k} = [a \times \{d_{P,k} + b\}^c + e] \times 10^8 \tag{45}$$

where a, b, c, and e are empirically determined constants which, for instance, for a white iron alloy were assessed [146] as $a = 4.236 \times 10^{14}$, $b = 490$, $c = -3.861$ and $e = 180$.

Gupta et al. [149] by doing a quantitative comparison of the erosion rate under different operating conditions developed a relationship between the maximum erosion rate and the main operating parameters which is given as:

$$E_T^{max} = K \left(\frac{d_P}{H_{ch}} \right)^{n_1} (C_{avg.})^{n_2} (Re_H)^{n_3} (\omega_H)^{n_4} \tag{46}$$

where d_P is the particle size; H_{ch} is the height of channel; $C_{avg.}$ is the mean slurry concentration; Re_H and ω_H are the Reynold number and rotational velocity for the channel height of H_{ch}, respectively. K, and n_i for $i = 1–4$ are empirical constants.

4.4. Closed-loop pipeline rig

A closed-loop pipeline test rig was described in detail for the first time in 1988 by Steward [151]. It is a popular test method for studying actual pipeline erosion as it can be designed to produce similar operating conditions to real pipelines. The five main components of the test rig are a slurry reservoir, centrifugal slurry pump, heat exchanger, jet nozzle and specimen holder. The solids are kept suspended by agitation within the galvanized iron slurry reservoir, which has a capacity of 1.8 m^3. The centrifugal slurry-handling pump is driven by a hydraulic variable-speed motor, and the velocity and concentration of the slurry could be monitored by means of a magnetic flowmeter and weigh tank, respectively. As the major part of the energy generated by the pump and friction is transferred to the slurry in the form of heat, mild steel heat exchangers are provided to remove the heat and maintain the temperature of the slurry in the system at approximately 25 °C. The jet nozzle, which is attached at the end of the return line, creates a jet impact erosion condition, which makes it possible to compare impact jet erosion test results and pipeline test results for the same test conditions. Flat samples are kept in place below the slurry jet by means of a holder to which they are bolted [151]. A schematic diagram of a typical closed-loop pipeline rig is given in Fig. 27. It has to be noted that as the duration of the test compared to other test methods is much longer, the slurry has to be periodically replaced to reduce the effect of particle degradation.

Several studies [152–158] have been made to develop physical or empirical models to describe the erosion process in straight pipes, elbows and ducts mainly using the following steps:

I. Flow pattern prediction under different velocities
II. Particle tracking
III. Erosion rate prediction

The two first steps are beyond the scope of this work and for more information readers are referred to the original literature [152–158]. Regarding the last step, it is worth noting that one of the initial empirical erosion equations suggested by Neilson and Gilchrist [159], which was later modified by Wallace et al. [161], is most commonly employed to predict the erosion rate (mg/g) in straight pipe. It has the form:

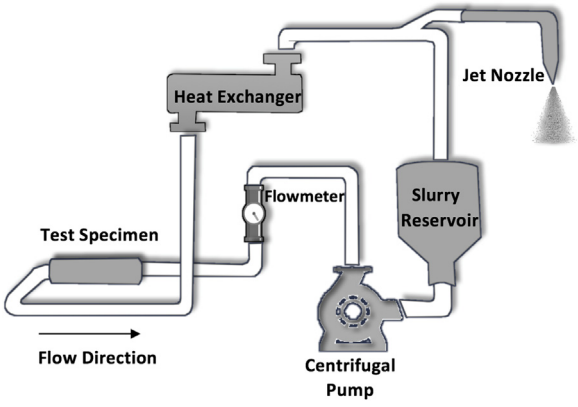

Fig. 27. Schematic illustration of a typical closed-loop pipeline rig.

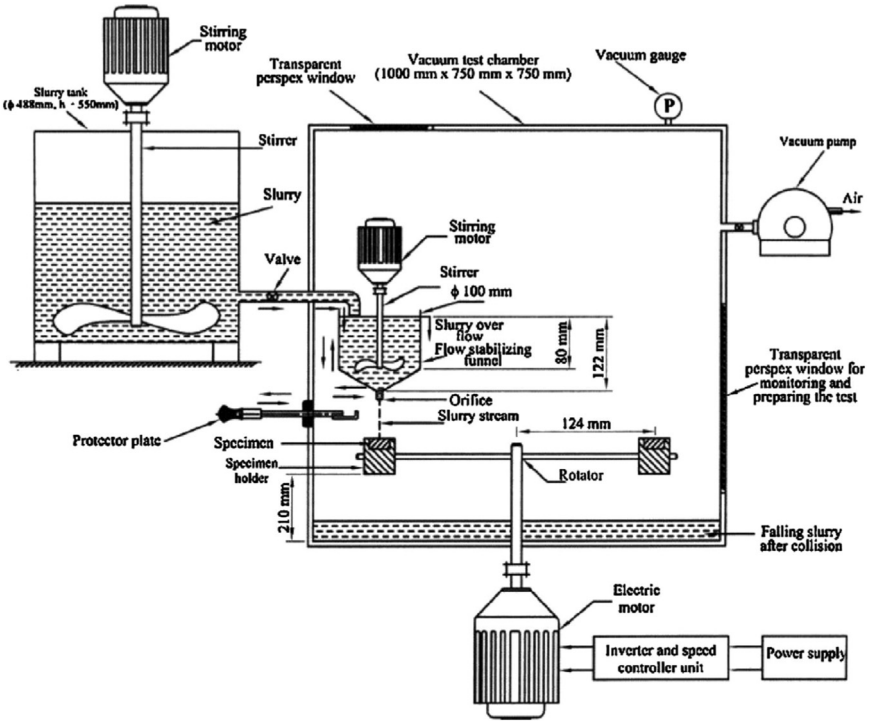

Fig. 28. Schematic diagram of the slurry erosion whirling-arm rig [58].

$$E_T = \begin{cases} \frac{1}{N_P}\left[\frac{1/2(V_p^2\cos^2\alpha\sin 2\alpha)}{\varepsilon} + \frac{1/2(V_P^2\sin^2\alpha)}{\Phi}\right], & \alpha \le 45° \\ \frac{1}{N_P}\left[\frac{1/2(V_p^2\cos^2\alpha)}{\varepsilon} + \frac{1/2(V_P^2\sin^2\alpha)}{\Phi}\right], & \alpha > 45° \end{cases} \quad (47)$$

where ε and Φ are the coefficients for the cutting and deformation erosion components. For carbon steel, they are reported to be 33,316.9 and 77,419.7, respectively [153–160]. N_P is the number of solid particles throughput.

Another commonly used model based on the stress field generated within the plastic deformation zone caused by particle impingements was proposed by Hashish [161] and later used by Wood et al. [154] for pipe bends. It is given in Eq. (48).

$$E_w = \left\{\frac{100}{2\sqrt{29}} r_P{}^3 \left(\frac{V_P}{C_K}\right)^n \sin 2\alpha\sqrt{\sin\alpha}\right\} + \left\{\frac{M_P(V_P\sin\alpha - D_K)^2}{2\Phi}\right\} \quad (48)$$

where r_P, V_P, M_P are respectively the particle radius (m), velocity (m s^{-1}) and mass (kg), C_K and D_K are cutting and deformation characteristic velocities (m s^{-1}) which are expressed as:

$$C_K = \sqrt{\frac{3\sigma_T R_f{}^{0.6}}{\rho_P}} \quad (49)$$

and

$$D_K = \frac{\pi^2}{2\sqrt{10}}(1.59Y_s)^{2.5}\left(\frac{R_f}{\rho_T}\right)^{0.5}\left[\frac{1-\nu_P{}^2}{E_P} + \frac{1-\nu_T{}^2}{E_t}\right]^2 \quad (50)$$

where σ_T is the plastic flow stress (N m^{-2}), ρ_T is density (kg m^{-3}), ν_T is Poisson's ratio, E_t is Young's modulus (N m^{-2}), and Y_s is the yield stress (N m^{-2}) of the target material. For the particles, ρ_P is density (kg m^{-3}), ν_P is Poisson's ratio, E_P is Young's modulus (N m^{-2}), R_f a roundness factor in the range 0–1. Hashish [161] reported an empirical value of n = 2.54 and $\Phi = 1.9\times10^{10}$ for AISI 4130.

Bourgoyne [162] proposed an empirical model based on a comprehensive experimental study using a closed-loop pipeline rig focusing on the influence of the carrier fluid nature on the erosion rate. For high flow velocities, the following relationships for estimating the rate of erosion caused by liquid-solid slurries were developed:

$$E_T = F_e \frac{\rho_P}{\rho_T}\frac{q_P}{A_{Pipe}}\left(\frac{V_{SL}}{100 f_l}\right)^2 \quad (51)$$

where F_e is a specific erosion factor which is defined as the mass of removed material per unit mass of erodent (kg/kg); A_{Pipe} is the pipe cross-sectional area (m^2); ρ_P, ρ_T are the density of solid particles and target material (kg/m^3), respectively; q_P is the flow rate of solid particles (m^3/s); V_{SL} are the superficial liquid velocity (m/s), and f_l is the volume fraction of liquid.

Zhang et al. [156] pointed out that during slurry transportation in a straight pipe, the flow field consisted of two regions, a core region of turbulent flow and a thin boundary layer. They stated that when the solid particles pass through the turbulent region, not all of them can reach and strike the pipe wall, as some of them can be trapped in the vortex flow. Therefore, instead of the actual particle mass an effective mass flow must be used for the erosion model. In accordance with this concept, after analyzing the random movement of the particles, they proposed that the total erosion rate in a long straight pipe caused by particle sizes ranging from 50 to 1000 μm can be well predicted using Oka's model (Eq. (14)) if impact velocity and impact angle are calculated as follows:

$$\begin{cases} V_P = \sqrt{v_{pt}^r{}^2 + v_p^{z2}} \\ \alpha = \tan^{-1}\frac{v_{pt}^r}{v_p^z} \end{cases} \quad (52)$$

where v_{pt}^r is the impact velocity in the radial direction which can be calculated as

$$v_{pt}^r = \eta_\delta v_p^r \quad (53)$$

and v_p^z is the axial component of the impact velocity. It is almost equal to the fluid velocity in the center of the vortex flow and is given by:

$$v_p^z \approx v_f^z\left(\frac{l_p}{2}\right) = V_m + 2.5v_* Ln\frac{l_p+2\delta}{D_P} + 3.75v_* \quad (54)$$

where v_p^r, v_f^z, v_* and V_m are the particle radial, fluid axial, friction

Table 3
Summary of erosion test rigs.

Test name	Advantages	Disadvantages	Test duration	Suitability to model building	Surface impact condition	Major parameters considered in resultant models
Slurry pot test	■ Simple in design and easy to manufacture and operate [162] ■ Simple and inexpensive test rig that can quickly rank of the erosion resistance of different materials [120] ■ Comparatively realistic results for many field applications [120]	■ Non-uniform distribution of solid particles and turbulence [117] ■ Effect of particle size, impact velocity and impact angle cannot be investigated without modification [120,164] ■ In test rigs without propellers, at more than 1600 rpm, vortex shedding interaction effects can appear between the two cylindrical samples [120]	Hours	Well-defined Geometry (Best for analytical modeling)	Controlled **average** particle impact angle and velocity	V_P, α, d_P, C_w,S_F, ρ_p, K_T, H_T, H_p
Jet Erosion Tester	■ Convenient and reproducible [63] ■ Easy control of impingement angle and velocity [163]	■ The impact angle and the impact velocity of all the solid particles do not remain the same during the test [117,163,164] ■ The impact velocity must be measured and calibrated periodically because of the wear of the nozzle ■ Possibility of local concentration of the slurry jet on the specimen surface [107]	Minutes - Hours	Straightforward (Best for CFD and semi-empirical modeling)	Controlled particle trajectory	V_P, α, d_P, S_F, ρ_P, M_P, H_T, P_{TR}, P_s, S_T, e_T
Coriolis erosion tester	■ Simple and rapid with excellent control of experimental conditions [139] ■ Good for reproducing the action of slurries moving inside centrifugal pumps and cyclones [140] ■ Good for ranking erosion resistance of slurry pump components [141]	■ Simulating the erosion just under low interaction intensity (Only low impingement angles and low velocities) [140] ■ Only suitable for flat samples	Minutes	Complicated geometry	Controlled **average** particle impact angle and velocity	V_P, α, d_P, C_w, ρ_P, M_P, u_P , τ_k, E_S, R_e, ω, V_{rp}, $F_{cent.}$, F_{dr},Q
Closed-loop pipeline rig	■ Very close to industrial conditions [107] regarding to achieve actual pipeline flow conditions [147]	■ High cost and time consuming [107] ■ High probability of damage to pump propeller after a short usage time, which causes variations in the flow velocity and actual slurry transfer rate, thereby reducing the reliability of the experimental results [75]	Days-Weeks	Easy to model especially for low solid concentrations	Flow direction is usually parallel to the surface (for straight pipes)	V_P, N_P, α, r_P, σ_T, R_f, ρ_P, ρ_T, Y_s, E_P, E_t, ν_P, ν_T, q_P, ν_{pt}^r, ν_p^z, l_p

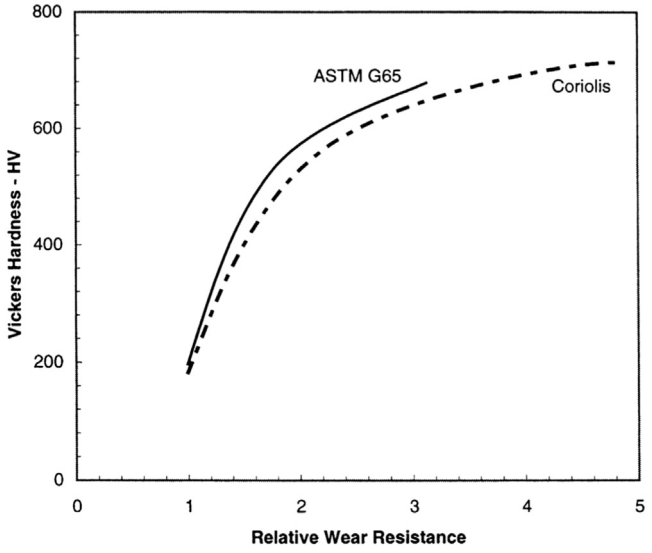

Fig. 29. Relative wear performance of AISI 1020 steel with the, Coriolis erosion test and ASTM G65 abrasion resistance test [35].

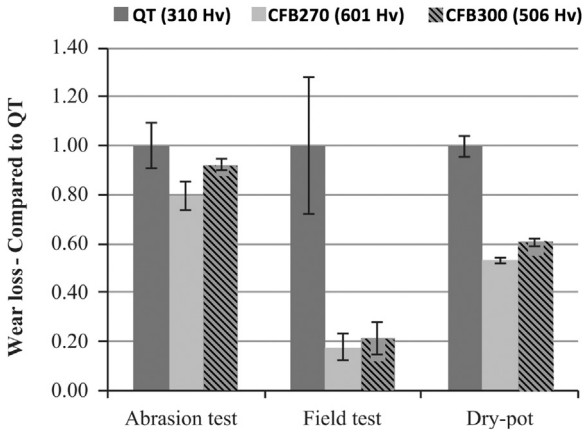

Fig. 30. Wear test results relative to a QT reference material [90].

velocity and mean velocity (m/s), respectively. η_δ is the attenuation coefficient (dimensionless); l_p is the particle displacement (m) which is defined as amount of particle movement after a random walk through the vortex flow to reach the target surface; D_P is the pipe diameter and δ is the boundary layer thickness (m).

4.5. Slurry whirling arm rig

There are some other test rigs, which have mostly been developed to simulate specific slurry erosion conditions rather than for erosion model development. The most important one is the slurry whirling rig and the sand blast type erosion tester.

The slurry whirling arm rig is a combination of a jet erosion tester and a slurry pot in which the sample is rotating while at the same time a jet of slurry impacts the sample surface. The test rig consists of three main parts: a) the specimen rotation unit which provides impact velocity by using a variable speed motor, two aligned arms, and two specimen holders, b) the slurry unit which delivers a homogeneous stable slurry stream, and c) the vacuum unit that is responsible for evacuating the slurry chamber to eliminate aerodynamic effects from the slurry system. A schematic illustration of a typical Whirling arm rig is given Fig. 28. As the specimen holders can be tilted and locked, the impact angle can be adjusted to a required value by rotating the specimen holder around its horizontal axis [29,58,163,164].

4.6. Summary of the test methods and erosion models

Erosion studies can be classified into two categories: i) experimental work to reveal erosion mechanisms and rank materials, and ii) investigations aimed at developing general theoretical, mechanistic, or empirical erosion models and simulation tools. Regarding the experimental studies, it has not been possible to give an extensive review of all available experimental slurry erosion test rigs. However, common to all is the use of erodent particles in different size ranges suspended in either a liquid or a gas. The most common particles are alumina, silicon carbide, quartz and ores. The purpose of all of the experimental approaches has been the generation of data that, on the one hand can increase our understanding of the fundamental erosion phenomena and, on the other hand, can be used to evaluate erosion damage and predict the behavior of different materials in real erosive systems. Selection of an appropriate test machine is necessary if the aim is to reproduce real service conditions. Table 3 summarizes some of the pros and cons of the reviewed most common test methods. Sometimes, if the aim is to simply rank materials relative to each other, the choice of test is less critical. Clark and Llewellyn [35] have shown that the relative wear performance of AISI 1020 heat treated to different hardness levels is very similar irrespective of whether the ranking is obtained by means of the Coriolis erosion test or by means of the ASTM G65 abrasion test, see Fig. 29. Nonetheless, selection of a proper test method that reproduces as closely as possible the real conditions experienced is crucial in evaluating actual material performance.

For example, Vuorinen and co-workers [90] conducted three different types of wear test on three different materials: 1) abrasion, 2) erosion using a high-speed dry pot tester, and 3) a real field test. Two carbide-free bainitic steels (in wt% 1.00C, 2.50Si, 0.75Mn, and 1.00Cr) produced with two austempering temperatures, 270 and 300 °C, named as CFB270 and CFB300 and a commercial quenched and tempered (QT) steel, which is generally used in industry for erosion applications (0.35C, 0.31Si, 0.72Mn, 1.00Cr, 1.36Ni, and 0.18Mo). The test results given in Fig. 30 show that while the general trends and ranking order of the materials in all the tests is the same, the abrasion test implies that there are no significant differences between the materials. On the other hand, large differences were found in the field test and these were better reproduced by the erosion test. This shows that the key to reliable performance evaluation requires the selection of a test rig based on an understanding of the actual wear mechanism.

Regarding the modeling studies, it has been shown that many investigations have been carried out to develop both physical and numerical erosion models by employing various experimental erosion test rigs. Since the early 1990s, CFD has also been widely used for this purpose. However, the complexity of the erosion phenomenon and the number of variables involved has made it challenging to obtain a generally applicable model. Almost all of the proposed models are essentially empirically based and consequently have some degree of dependence on empirical coefficients. Nonetheless, mainly using one of the models reviewed in this work, many attempts have been made with the aid of CFD to incorporate fluid flow and particle trajectory equations and predict not only the erosion rate but also the erosion pattern and penetration depth.

Considering some statistics from the reviewed equations, there are more than 20 equation constants and 30 different independent parameters, which are listed in Table 4 along with the power index of these parameters (if applicable). Table 5 gives the materials covered in the reviewed publications: almost 30 different steel compositions in addition to the other materials, both ductile and hard. Considering all the proposed models and empirical equations in this review, on average, they contain five parameters. Eq. (48) contains as many as 13 parameters while Eq. (27) considers only two parameters, i.e. particle impact velocity and angle. According to Table 4, the top 5 most frequently considered parameters are 1) particle impact velocity (44 times), 2) particle size (34 times), 3) particle impact angle (32 times), 4) slurry

Table 4
Summary of the parameters used in the reviewed equations and, where relevant, their powers for the various target materials considered.

Equation No.	Reference	Material Code (Table 5)	1-Target material hardness	2-Particle mass	3-Particle size (d_P)	4-Particle velocity	5-Impact angle	6-Slurry concentration	7-Particle density	8-Target material density	9-Particle shape	10-Impact angle function $f(\alpha)$	11-Target material toughness	12-Critical strain (ε_{cr})	13-Particle fragmentation	14-Target material Poisson ratio	15-Particle Poisson ratio	16-Ratio of the hardness (H_T/H_P)	17- Microstructure	18-Particle restitution	19-Slurry fluid density	20-Target material flow pressure	21-Rotational speed	22- Work hardening	23-Target material stiffness	24-Target material elongation	25-Particle Young modulus	26-Target material Young modulus	27-Target material yield stress	28- Target material shear stress	29-Particle tangential velocity	30-Sliding specific energy
2	17	4,24, 19,3, 36		✓	✓	2.0	✓																									
2	27	21			2.0																										
2	27	31			4.0																										
12	53	32			3.0	2.0						✓			✓																
16*	114	21	-1.5		3.0	3.0	✓		1.5																						
16*	114	41	-1.5		3.0	3.0	✓		1.5																						
16	46	27			0.29	2.48		0.51																							
16	46	35			0.34	2.14		0.55																							
16	47	27			0.85	2.56		0.83																							
16*	41	14			3.0	2.1																									
16*	72	27				2.62																									
16*	65	14				2.53		0.72																							
16*	72	40				2.64-2.94																									
16*	171	2,9				2.0																									
17	89	19			1.37	3.5	0.1	1.09																							
17	24	3,10, 25,26			✓	✓		✓											✓												
17	34	14,15, 19,22, 30,35			✓	✓		✓			✓							✓														
18	122	1, 5-7, 37	-1.0		2.0								-2.0			✓															
19*	41	31			4.0	2.37				0.9								-0.46													
19	128 132	14,19 30,35			1.62	2.02		-0.28										✓													
20	128 132	14,19 30,35	-0.7		1.55	2.35		-0.11			✓	✓																			
24	133	14,16, 20,38				2.0	✓					✓								✓											
27	134	28				2.5						✓																			
28	127	29			0.66	2.39	✓	0.68										0.26, 3.81													
29	172	15	-0.59			2.4	✓				✓																				
29*	173	23	✓		0.2	2.6																									
29	56	35	-0.15			3.0			0.5	1.0		✓																			
29	60	15	-0.59			2.4					✓	✓																			
29	136	28	-0.59			1.73					✓	✓																			
32	39	11,12, 15,18		✓		✓		✓			✓	✓										✓		✓							
32	88	14		✓		4.09						✓																			
32*	54	42		✓		2.25						✓																			
34	106	14,19, 28,30	✓		✓	✓						✓																			
34	174 175	14	✓		✓	✓						✓																			
34	103	14,19, 28-30	✓		✓	✓						✓																			
35	130	8, 19, 30			0.5	2.37			0.2			✓		✓								✓		✓							
36	65	28	-0.7	1.1	✓	2.25																			✓	✓					
37	116	35		✓	✓				✓												✓		✓								
40	145	4			✓	✓	✓	✓	✓														✓								
40	142	4,21, 34				✓		✓															✓								
43 44	150	29			✓	3.0	✓	1.0		✓																			✓	✓	✓
43 44	146	39			✓	3.0	✓	1.0		✓																			✓	✓	✓
47	176	19,31			✓	2.0	✓					✓																			
47	160	28			✓	2.0	✓					✓																			
48	154	14		✓	✓	2.54	✓		✓	✓	✓					✓	✓					✓					✓	✓	✓			
48	161	28		✓	✓	2.54	✓		✓	✓	✓					✓	✓					✓					✓	✓	✓			
48	177	35		1.0	✓	2.0	✓		✓	✓	✓					✓	✓					✓					✓	✓	✓			

* : Almost similar

concentration (15 times) and 4) target material hardness (14 times).

For both brittle and ductile materials, the mean value of the power of the particle velocity is 2.45. This compares with the value of 2 expected on the basis of the kinetic energy of the impacting particle, i.e. $\frac{1}{2}mV_P^2$. The minimum value is 1.73 (Eq. (29) for ASTM A216 carbon steel) while the maximum value exceeds 4 (Eq. (32) for AISI 304). However, the powers of particle size, impact angle, hardness and slurry concentration vary considerably between the equations, being sensitive to the particle and material properties and the test conditions. However, in the case of power law relationships between the total erosion

Table 5
Material codes used in Table 4.

No.	Material	No.	Material
1	AISI 1010	22	Aluminum alloy 6063
2	AISI 10105	23	AISI H13 (tool steel)
3	AISI 1018	24	API P110 (casting steel)
4	AISI 1020 (hot rolled steel)	25	API X42
5	AISI 1030	26	API X70
6	AISI 1040	27	Brass
7	AISI 1050	28	Carbon Steel
8	AISI 1055	29	Cast iron
9	AISI 1078	30	Copper
10	AISI 1080	31	Glass (Pyrex)
11	AISI 2101	32	H46 steel (11% chromium steel)
12	AISI 2205	33	Inconel 625
13	AISI 2507	34	M2 tool steel
14	AISI 304 (L)	35	Mild steel
15	AISI 316(L)	36	OFHC copper
16	AISI 410	37	Steel 50CrV4
17	AISI 4130	38	Ti-6Al-4V
18	AISI 904(L)	39	White iron
19	Aluminum	40	0.6% C Martensitic steel
20	Aluminum alloy 2024	41	5 different type of Stellite alloys
21	Aluminum alloy 6061	42	12 different type of metals mostly carbon and stainless steel

rate and the variables, Table 4 gives a good picture of the power indices for the parameters concerned, covering a range of steel compositions and test methods.

In a nutshell, no single definitive model describing slurry erosion currently exists; rather, numerous qualitative and quantitative models have been proposed.

5. Concluding remarks and future work

The economic importance of slurry erosion and the significant operating problems that it produces in different applications have led to many investigations that consider the erosion of metals from various aspects. These cover the design and improvement of test rigs, understanding basic mechanisms, simulating actual processes, and the development of analytical models to predict the erosion rate in different applications. The majority of these works have been conducted to study the effect of different parameters on slurry erosion and its mechanisms using several test methods including various laboratory or pilot test rigs. There is no generally accepted universal test method for evaluating and comprehensively studying slurry erosion. One of the main reasons is the fact that the severity of erosion damage is greatly affected not only by differences in the nature and condition of the abrasive media and the target material properties but also by the characteristics of the carrier fluid flow. Therefore, despite expectations in industry, it is not possible to estimate the erosion performance of materials by doing a single test. Thus, it is necessary to conduct several evaluations varying from microstructure observations to the measurement of various mechanical properties to provide comprehensive information for evaluation of the erosion behavior of materials in a specific application.

Regarding the effect of microstructure, some efforts have been made to address what is occurring microstructurally during erosion by using scanning electron microscopy (SEM), but there is still a lack of systematic work on microstructure evaluation during the erosion process by using other methods such as SEM-EBSD (electron backscatter diffraction) and TEM (transmission electron microscopy) in order to reveal more microstructural features such as the disintegration of martensite boundaries, low-angle grain boundaries, dislocation structure, and misorientation analysis of plastic deformation.

The observation of worn surface morphologies has shown that cutting and ploughing processes are the main forms of material removal in ductile materials, while micro-crack formation and deformation are the main mechanisms of erosion in brittle materials. Apart from the properties of the eroded and erosive materials, particle impact characteristics including particle impact velocity and impact angle are the most important parameters affecting the erosion.

There is a general agreement in the ranking of steels with regard to erosion resistance [35,39,119] that the lowest erosion resistance is found in single-phased austenitic or ferritic steels. Erosion resistance increases with an increasing share of pearlite or bainite in the microstructure. In the martensitic steels or dual phase steels (martensite + ferrite), the presence of carbides in the martensitic matrix could lead to a further increase of erosion resistance. It has been shown that for a given chemical composition, the erosion resistance of different microstructures also depends on the distribution of the different individual microstructural constituents in the matrix and sometimes it is not what would have been expected on the basis of macroscopic hardness alone. For instance, in some cases, a spheroidized steel offered a lower erosion rate than a fine pearlitic microstructure with a higher hardness or even a harder martensitic microstructure. However, in most instances, martensite is the preferred microstructure when improved erosion and abrasion resistance is required.

Improvement of the common erosion resistant steels, and modification of service parameters are sometimes insufficient solutions to slurry erosion. Other strategies should also be considered. Thus, in order to minimize the erosion rate in some special applications, researchers have used various surface treatments to enhance the erosion resistance, such as carburizing [163], hardfacing [165], or ceramic coating [166]; or employed new production methods such as thermo-mechanical control processing [167,168] or even developed new materials like composites and cermets [105,169,170].

The evaluation of erosion under different erosive conditions using erosion test rigs is very expensive and time consuming, especially for the industrial pilot plant tests. In addition, the results can only be applied to the same conditions as used in the tests. Hence, nowadays many investigations have been conducted to develop a methodology for predicting the erosion rate from empirical relations for slurry erosion. Although this approach is ongoing and there is still much to achieve before a comprehensive model is obtained, progress so far is satisfactory.

Owing to the wide variety and increasing numbers of applications suffering from erosion, the future will be extremely challenging for surface engineers. Based on the studies conducted so far, it seems that the following topics should help to pave the way ahead:

- Consideration of the possible transition in the target material from ductile to brittle behavior during the course of the erosion process may be a key factor in improving the applicability of short-term test predictions to real erosion situations.
- It would be interesting to study the relationship between erosion and target material low-cycle fatigue properties, as such considerations have not yet been investigated.
- Taking account of particle–particle interactions, which have been ignored until now, could offer possibilities for more accurate and widely applicable models.
- From the pipeline point of view, as almost all industrial pipes are made from rolled plate, there is an obvious lack of studies concerning the effects of crystallographic texture on erosion. This could be an interesting topic for the future studies that might lead to a refined understanding regarding the influence of the target material.
- The changes in the stress distribution and micro-texture in the eroded surfaces as a result of the erosion process could help in the development of erosion resistant materials.
- The effect of temperature on erosion rate needs more studies. This would be useful in predicting erosion at elevated temperatures, e.g. in chemical plants.

Acknowledgment

The authors are grateful for financial support from the European Commission under grant number 675715 – MIMESIS – H2020-MSCA-ITN-2015, which is a part of the Marie Sklodowska-Curie Innovative Training Networks European Industrial Doctorate Programme.

References

[1] R.J. Llewellyn, S.K. Yick, K.F. Dolman, Scouring erosion resistance of metallic materials used in slurry pump service, Wear 256 (2004) 592–599, http://dx.doi.org/10.1016/j.wear.2003.10.002.
[2] R. Hamzah, D.J. Stephenson, J.E. Strutt, Erosion of material used in petroleum production, Wear 186–187 (1995) 493–496, http://dx.doi.org/10.1016/0043-1648(95)07127-X.
[3] F. Aiming, L. Jinming, T. Ziyun, Failure analysis of the impeller of a slurry pump subjected to corrosive wear, Wear 181–183 (1995) 876–882, http://dx.doi.org/10.1016/0043-1648(95)90210-4.
[4] R. Macchini, M.S.A. Bradley, T. Deng, Influence of particle size, density, particle concentration on bend erosive wear in pneumatic conveyors, Wear 303 (2013) 21–29, http://dx.doi.org/10.1016/j.wear.2013.02.014.
[5] I. Finnie, Erosion of surfaces by solid particles, Wear 3 (1960) 87–103, http://dx.doi.org/10.1016/0043-1648(60)90055-7.
[6] J.G.A. Bitter, A study of erosion phenomena, Wear 6 (1963) 169–190, http://dx.doi.org/10.1016/0043-1648(63)90073-5.
[7] P.E. Grobler, R.J. Mostert, Experience in the laboratory and commercial development of abrasion-corrosion resistant steels for the mining industry, Wear 135 (1990) 339–354, http://dx.doi.org/10.1016/0043-1648(90)90035-9.
[8] B.W. Madsen, Measurement of erosion-corrosion synergism with a slurry wear test apparatus, Wear 123 (1988) 127–142, http://dx.doi.org/10.1016/0043-1648(88)90095-6.
[9] N. Ojala, K. Valtonen, A. Antikainen, A. Kemppainen, J. Minkkinen, O. Oja, V. Kuokkala, Wear performance of quenched wear resistant steels in abrasive slurry erosion, Wear 354–355 (2016) 21–31, http://dx.doi.org/10.1016/j.wear.2016.02.019.
[10] B.E.A. Jacobs, Design of Slurry Transport Systems, Elsevier Science Publishers Ltd, London, 2005.
[11] Y. Li, G.T. Burstein, I.M. Hutchings, The influence of corrosion on the erosion of aluminium by aqueous silica slurries, Wear 186–187 (1995) 515–522, http://dx.doi.org/10.1016/0043-1648(95)07181-4.
[12] S.S. Rajahram, T.J. Harvey, R.J.K. Wood, Evaluation of a semi-empirical model in predicting erosion – corrosion, Wear 267 (2009) 1883–1893, http://dx.doi.org/10.1016/j.wear.2009.03.002.
[13] I. Finnie, Some observations on the erosion of ductile metals, Wear 19 (1972) 81–90, http://dx.doi.org/10.1016/0043-1648(72)90444-9.
[14] G.F. Truscott, A literature survey on abrasive wear in hydraulic machinery, Wear 20 (1972) 29–50, http://dx.doi.org/10.1016/0043-1648(72)90285-2.
[15] P.P. Shitole, S.H. Gawande, G.R. Desale, B.D. Nandre, Effect of impacting particle kinetic energy on slurry erosion wear, J. Bio-Tribo-Corros. 1 (2015) 29, http://dx.doi.org/10.1007/s40735-015-0028-6.
[16] S.L. Sinha, S.K. Dewangan, A. Sharma, A review on particulate slurry erosive wear of industrial materials: In context with pipeline transportation of mineral – slurry, Part. Sci. Technol. 6351 (2015) 1–16, http://dx.doi.org/10.1080/02726351.2015.1131792.
[17] H.M. Clark, K.K. Wong, Impact angle, particle energy and mass loss in erosion by dilute slurries, Wear 186–187 (1995) 454–464, http://dx.doi.org/10.1016/0043-1648(95)07120-2.
[18] Y.F. Wang, Z.G. Yang, Finite element model of erosive wear on ductile and brittle materials, Wear 265 (2008) 871–878, http://dx.doi.org/10.1016/j.wear.2008.01.014.
[19] M. Parsi, K. Najmi, F. Najafifard, S. Hassani, B.S. McLaury, S.A. Shirazi, A comprehensive review of solid particle erosion modeling for oil and gas wells and pipelines applications, J. Nat. Gas Sci. Eng. 21 (2014) 850–873, http://dx.doi.org/10.1016/j.jngse.2014.10.001.
[20] I. Finnie, G.R. Stevick, J.R. Ridgely, The influence of impingement angle on the erosion of ductile metals by angular abrasive particles, Wear 152 (1992) 91–98, http://dx.doi.org/10.1016/0043-1648(92)90206-N.
[21] A.V. Levy, The solid particle erosion behavior of steel as a function of microstructure, Wear 68 (1981) 269–287, http://dx.doi.org/10.1016/0043-1648(81)90177-0.
[22] A. Islam, Z.N. Farhat, Effect of impact angle and velocity on erosion of API X42 pipeline steel under high abrasive feed rate, Wear (2014) 1–11, http://dx.doi.org/10.1016/j.wear.2014.01.005.
[23] M. Barge, G. Kermouche, P. Gilles, J.M. Bergheau, Experimental and numerical study of the ploughing part of abrasive wear, Wear 255 (2003) 30–37, http://dx.doi.org/10.1016/S0043-1648(03)00159-5.
[24] T. Alam, M. Aminul Islam, Z.N. Farhat, Slurry erosion of pipeline steel: effect of velocity and microstructure, J. Tribol. 138 (2015) 21604, http://dx.doi.org/10.1115/1.4031599.
[25] G. Sundararajan, M. Roy, B. Venkataraman, erosion efficiency – a new parameter to characterise the dominant erosion micromechanism, Wear 140 (1990) 369–381.
[26] H.S. Grewal, A. Agrawal, H. Singh, Identifying erosion mechanism: a novel approach, Tribol. Lett. 51 (2013) 1–7, http://dx.doi.org/10.1007/s11249-013-0156-4.
[27] H.M. Clark, R.B. Hartwich, A re-examination of the “particle size effect” in slurry erosion, Wear 248 (2001) 147–161, http://dx.doi.org/10.1016/S0043-1648(00)00556-1.
[28] C.I. Walker, M. Hambe, Influence of particle shape on slurry wear of white iron, Wear 332–333 (2015) 1021–1027, http://dx.doi.org/10.1016/j.wear.2014.12.029.
[29] A. Kasem, Particle size effects on slurry erosion of 5117 steels, J. Tribol. 133 (2011) 1–7, http://dx.doi.org/10.1115/1.4002605.
[30] M. Liebhard, A. Levy, Effect of erodent particle characteristics on the erosion of metals, Wear 151 (1991) 381–390, http://dx.doi.org/10.1016/0043-1648(91)90263-T.
[31] A. Yabuki, K. Matsuwaki, M. Matsumura, Critical impact velocity in the solid particles impact erosion of metallic materials, Wear 233–235 (1999) 468–475, http://dx.doi.org/10.1016/S0043-1648(99)00170-2.
[32] A.V. Levy, P. Chik, The effects of erodent composition and shape on the erosion of steel, Wear 89 (1983) 151–162, http://dx.doi.org/10.1016/0043-1648(83)90240-5.
[33] H. Arabnejad, S.A. Shirazi, B.S. Mclaury, H.J. Subramani, L.D. Rhyne, The effect of erodent particle hardness on the erosion of stainless steel, Wear 333 (2015) 1098–1103, http://dx.doi.org/10.1016/j.wear.2015.01.017.
[34] G.R. Desale, B.K. Gandhi, S.C. Jain, Slurry erosion of ductile materials under normal impact condition, Wear 264 (2008) 322–330, http://dx.doi.org/10.1016/j.wear.2007.03.022.
[35] H.M. Clark, R. Llewellyn, Assessment of the erosion resistance of steels used for slurry handling and transport in mineral processing applications, Wear 250 (2001) 32–44, http://dx.doi.org/10.1016/S0043-1648(01)00628-7.
[36] H. Arabnejad, A. Mansouri, S.A. Shirazi, B.S. McLaury, Development of mechanistic erosion equation for solid particles, Wear 332–333 (2015) 1044–1050, http://dx.doi.org/10.1016/j.wear.2015.01.031.
[37] Y.I. Oka, M. Nishimura, K. Nagahashi, M. Matsumura, Control and evaluation of particle impact conditions in a sand erosion test facility, Wear 250–251 (2001) 736–743, http://dx.doi.org/10.1016/S0043-1648(01)00710-4.
[38] M. Vite-Torres, J.R. Laguna-Camacho, R.E. Baldenebro-Castillo, E.A. Gallardo-Hernández, E.E. Vera-Cárdenas, J. Vite-Torres, Study of solid particle erosion on AISI 420 stainless steel using angular silicon carbide and steel round grit particles, Wear 301 (2013) 383–389, http://dx.doi.org/10.1016/j.wear.2013.01.071.
[39] M. Lindgren, J. Perolainen, Slurry pot investigation of the influence of erodent characteristics on the erosion resistance of austenitic and duplex stainless steel grades, Wear 319 (2014) 38–48, http://dx.doi.org/10.1016/j.wear.2014.07.006.
[40] A. Yabuki, M. Matsumura, Theoretical equation of the critical impact velocity in solid particles impact erosion, Wear 233–235 (1999) 476–483, http://dx.doi.org/10.1016/S0043-1648(99)00170-2.
[41] Z. Feng, A. Ball, The erosion of four materials using seven erodents – towards an understanding, Wear 233–235 (1999) 674–684, http://dx.doi.org/10.1016/S0043-1648(99)00176-3.
[42] E.P. Cox, A method of assigning numerical and percentage values to the degree of roundness of sand grains, J. Paleontol. 1 (1927) 179–183 ⟨https://www.jstor.org/stable/1298056?seq=1#page_scan_tab_contents⟩.
[43] A. Rathod, S.G. Sapate, R.K. Khatirkar, Shape factor analysis of abrasive particles used in slurry abrasion testing, Int. J. Mech. Ind. Eng. 2 (2012) 35–39.
[44] G.F. Vander Voort, Metallography: Principles and Practice, ASM International, 1984, http://dx.doi.org/10.1361/mpa https://www.asminternational.org/materials-resources/results/-/journal_content/56/10192/06785G/PUBLICATION.
[45] G.R. Desale, B.K. Gandhi, S.C. Jain, Particle size effects on the slurry erosion of aluminium alloy (AA 6063), Wear 266 (2009) 1066–1071, http://dx.doi.org/10.1016/j.wear.2009.01.002.
[46] R. Gupta, S.N. Singh, V. Sehadri, Prediction of uneven wear in a slurry pipeline on the basis of measurements in a pot tester, Wear 184 (1995) 169–178, http://dx.doi.org/10.1016/0043-1648(94)06566-7.
[47] B.K. Gandhi, S.N. Singh, V. Seshadri, Study of the parametric dependence of erosion wear for the parallel flow of solid-liquid mixtures, Tribol. Int. 32 (1999) 275–282, http://dx.doi.org/10.1016/S0301-679X(99)00047-X.
[48] H.M. Clark, The influence of the flow field in slurry erosion, Wear 152 (1992) 223–240, http://dx.doi.org/10.1016/0043-1648(92)90122-O.
[49] B.K. Gandhi, S.V. Borse, Nominal particle size of multi-sized particulate slurries for evaluation of erosion wear and effect of fine particles, Wear 257 (2004) 73–79, http://dx.doi.org/10.1016/j.wear.2003.10.013.
[50] M. Divakar, V.K. Agarwal, S.N. Singh, Effect of the material surface hardness on the erosion of AISI316, Wear 259 (2005) 110–117, http://dx.doi.org/10.1016/j.wear.2005.02.004.
[51] G.L. Sheldon, Effects of surface hardness and other material properties on erosive wear of metals by solid particles, J. Eng. Mater. Technol. 99 (1977) 133, http://dx.doi.org/10.1115/1.3443422.
[52] M. Naim, S. Bahadur, Effect of microstructure and mechanical properties on the erosion of 18 Ni (250) maraging steel, Wear 112 (1986) 217–234, http://dx.doi.org/10.1016/0043-1648(86)90242-5.
[53] G.P. Tilly, A two stage mechanism of ductile erosion, Wear 23 (1973) 87–96, http://dx.doi.org/10.1016/0043-1648(73)90044-6.
[54] E. Akbarzadeh, E. Elsaadawy, A.M. Sherik, J.K. Spelt, M. Papini, The solid particle erosion of 12 metals using magnetite erodent, Wear 282–283 (2012) 40–51, http://dx.doi.org/10.1016/j.wear.2012.01.021.
[55] A.N.J. Stevenson, I.M. Hutchings, Scaling laws for particle velocity in the gas-blast erosion test, Wear 181–183 (1995) 56–62, http://dx.doi.org/10.1016/0043-1648(95)90008-X.
[56] J.G. Mbabazi, T.J. Sheer, R. Shandu, A model to predict erosion on mild steel surfaces impacted by boiler fly ash particles, Wear 257 (2004) 612–624, http://dx.doi.org/10.1016/j.wear.2004.03.007.
[57] I.M. Hutchings, R.E. Winter, The erosion of ductile metals by spherical particles, J. Phys. D. Appl. Phys. 8 (1975) 8–14, http://dx.doi.org/10.1088/0022-3727/8/1/010.
[58] M.A. Al-Bukhaiti, S.M. Ahmed, F.M.F. Badran, K.M. Emara, Effect of impingement angle on slurry erosion behaviour and mechanisms of 1017 steel and high-chromium white cast iron, Wear 262 (2007) 1187–1198, http://dx.doi.org/10.1016/j.

wear.2006.11.018.
[59] W. Tsai, J.A.C. Humphrey, I. Cornet, A.V. Levy, Experimental measurement of accelerated erosion in a slurry pot tester, Wear 68 (1981) 289–303, http://dx.doi.org/10.1016/0043-1648(81)90178-2.
[60] A. Mansouri, S.A. Shirazi, B.S. Mclaury, Experimental and numerical investigation of the effect of viscosity and particle size on the erosion damage caused by solid particles, in: Proceedings of the FEDSM2014, Chicago, Illinois, USA, 2014, pp. 1–10.
[61] N.R. Kesana, J.M. Throneberry, B.S. McLaury, S.A. Shirazi, E.F. Rybicki, Effect of particle size and liquid viscosity on erosion in annular and slug flow, J. Energy Resour. Technol. 136 (2013) 12901, http://dx.doi.org/10.1115/1.4024857.
[62] K. Kowsari, D.F. James, M. Papini, J.K. Spelt, The effects of dilute polymer solution elasticity and viscosity on abrasive slurry jet micro-machining of glass, Wear 309 (2014) 112–119, http://dx.doi.org/10.1016/j.wear.2013.11.011.
[63] T. Frosell, M. Fripp, E. Gutmark, Investigation of slurry concentration effects on solid particle erosion rate for an impinging jet, Wear 342–343 (2015) 33–43, http://dx.doi.org/10.1016/j.wear.2015.08.003.
[64] S. Turenne, M. Fiset, J. Masounave, The effect of sand concentration on the erosion of materials by a slurry jet, Wear 133 (1989) 95–106, http://dx.doi.org/10.1016/0043-1648(89)90116-6.
[65] M.-H. Wang, C. Huang, K. Nandakumar, P. Minev, J. Luo, S. Chiovelli, Computational fluid dynamics modelling and experimental study of erosion in slurry jet flows, Int. J. Comput. Fluid Dyn. 23 (2009) 155–172, http://dx.doi.org/10.1080/10618560902744412.
[66] A. Levy, Y.-F. Man, Elevated temperature erosion-corrosion of 9Cr-1Mo steel, Wear 111 (1986) 135–159, http://dx.doi.org/10.1016/0043-1648(86)90216-4.
[67] J.A. Humphrey, Fundamentals of fluid motion in erosion by solid particle impact, Int. J. Heat Fluid Flow. 11 (1990) 170–195, http://dx.doi.org/10.1016/0142-727X(90)90036-B.
[68] C.E. Smeltzer, M.E. Gulden, W.A. Compton, Mechanisms of metal removal by impacting dust particles, J. Basic Eng. 92 (1970) 639, http://dx.doi.org/10.1115/1.3425091.
[69] J.P. Young, A.W. Ruff, Particle erosion measurements on metals, J. Eng. Mater. Technol. 99 (1977) 121, http://dx.doi.org/10.1115/1.3443420.
[70] G.R. Desale, B.K. Gandhi, S.C. Jain, Effect of erodent properties on erosion wear of ductile type materials, Wear 261 (2006) 914–921, http://dx.doi.org/10.1016/j.wear.2006.01.035.
[71] E. Kosa, A. Göksenli, Effect of impact angle on erosive abrasive wear of ductile and brittle materials, Int. J. Mech. Aerosp. Ind. Mechatron. Manuf. Eng. 9 (2015) 1588–1592 (scholar.waset.org/1999.8/10002428).
[72] B.A. Lindsley, A.R. Marder, The effect of velocity on the solid particle erosion rate of alloys, Wear 225–229 (1999) 510–516, http://dx.doi.org/10.1016/S0043-1648(99)00085-X.
[73] N. Ojala, K. Valtonen, P. Kivikytö Reponen, P. Vuorinen, V.T. Kuokkala, High speed slurry-pot erosion wear testing with large abrasive particles, Tribol. – Finn. J. Tribol. 33 (2015) 36–44.
[74] M.A. Islam, T. Alam, Z.N. Farhat, A. Mohamed, A. Alfantazi, Effect of microstructure on the erosion behavior of carbon steel, Wear 332–333 (2015) 1080–1089, http://dx.doi.org/10.1016/j.wear.2014.12.004.
[75] P.C. Okonkwo, A.M.A. Mohamed, E. Ahmed, Influence of particle velocities and impact angles on the erosion mechanisms of AISI 1018 steel, Adv. Mater. Lett. 6 (2015) 653–659, http://dx.doi.org/10.5185/amlett.2015.5645.
[76] X. Xu, S. Van der Zwaag, W. Xu, The effect of ferrite-martensite morphology on the scratch and abrasive wear behaviour of a dual phase construction steel, Wear 348–349 (2016) 148–157, http://dx.doi.org/10.1016/j.wear.2015.12.005.
[77] R. Li, X. Zuo, Y. Hu, Z. Wang, D. Hu, Microstructure and properties of pipeline steel with a ferrite / martensite dual-phase microstructure, Mater. Charact. 62 (2011) 801–806, http://dx.doi.org/10.1016/j.matchar.2011.05.013.
[78] Y. Hu, X. Zuo, R. Li, Z. Zhang, Effect of initial microstructures on the properties of ferrite-martensite dual-phase pipeline steels with strain-based design, Mater. Res. 15 (2012) 317–322, http://dx.doi.org/10.1590/S1516-14392012005000021.
[79] A. Sharma, A. Kumar, R. Tyagi, Erosive wear analysis of medium carbon dual phase steel under dry ambient condition, Wear 334–335 (2015) 91–98, http://dx.doi.org/10.1016/j.wear.2014.12.005.
[80] O.P. Modi, P. Pandit, D.P. Mondal, B.K. Prasad, A.H. Yegneswaran, A. Chrysanthou, High-stress abrasive wear response of 0.2% carbon dual phase steel: effects of microstructural features and experimental conditions, Mater. Sci. Eng. A 458 (2007) 303–311, http://dx.doi.org/10.1016/j.msea.2006.12.083.
[81] A. Bayram, A. Uguz, Effect of microstructure on the wear behaviour of a dual phase steel, Materwiss. Werksttech. 252 (2001) 249–252.
[82] M. Sawa, D.A. Rigney, Sliding behavior of dual phase steels in vacuum and in air, Wear 119 (1987) 369–390, http://dx.doi.org/10.1016/0043-1648(87)90042-1.
[83] L.K. Ji, H.L. Li, H.T. Wang, J.M. Zhang, W.Z. Zhao, H.Y. Chen, Y. Li, Q. Chi, Influence of dual-phase microstructures on the properties of high strength grade line pipes, J. Mater. Eng. Perform. (2014) 1–8, http://dx.doi.org/10.1007/s11665-014-1184-4.
[84] D.B. Rosado, W. De Waele, D. Vanderschueren, Latest developments in mechanical properties and metallurgical features of high strength line pipe steels, in: Proceedings of the Sustainable Construction and Design, Ghent, 2013, pp. 1–10. 〈https://dx.doi.org/10.13140/2.1.4498.5287〉.
[85] X. Zuo, Z. Zhou, Study of pipeline steels with acicular ferrite microstructure and ferrite-bainite dual-phase microstructure, Mater. Res. 18 (2015) 36–41, http://dx.doi.org/10.1590/1516-1439.256813.
[86] I. Nobuyuki, S. Nobuo, K. Joe, Development of ultra-high strength linepipes with dual-phase microstructure for high strain application, JFE Tech. Rep. 12 (2008) 15–19.
[87] X. Ji, X. Han, M. Zhou, J. Liu, Effect of heat treatment on the slurry erosion resistance of high strength steel DP980, Int. J. Mater. Res. 105 (2014) 1–6, http://dx.doi.org/10.3139/146.111042.
[88] Q.B. Nguyen, C.Y.H. Lim, V.B. Nguyen, Y.M. Wan, B. Nai, Y.W. Zhang, M. Gupta, Slurry erosion characteristics and erosion mechanisms of stainless steel, Tribol. Int. 79 (2014) 1–7, http://dx.doi.org/10.1016/j.triboint.2014.05.014.
[89] M.S. Patil, E.R. Deore, R.S. Jahagirdar, S.V. Patil, Study of the parameters affecting erosion wear of ductile material in solid-liquid mixture, in: Proceedings of the World Congress on Engineering, London, 2011.
[90] E. Vuorinen, N. Ojala, V. Heino, C. Rau, C. Gahm, Erosive and abrasive wear performance of carbide free bainitic steels – comparison of field and laboratory experiments, Tribol. Int. 98 (2016) 108–115, http://dx.doi.org/10.1016/j.triboint.2016.02.015.
[91] P.H. Shipway, S.J. Wood, A.H. Dent, The hardness and sliding wear behaviour of a bainitic steel, Wear 203–204 (1997) 196–205, http://dx.doi.org/10.1016/S0043-1648(96)07411-X.
[92] R. Rementeria, I. García, M.M. Aranda, F.G. Caballero, Reciprocating-sliding wear behavior of nanostructured and ultra-fine high-silicon bainitic steels, Wear 338–339 (2015) 202–209, http://dx.doi.org/10.1016/j.wear.2015.06.011.
[93] A. Leiro, E. Vuorinen, K.G. Sundin, B. Prakash, T. Sourmail, V. Smanio, F.G. Caballero, C. Garcia-Mateo, R. Elvira, Wear of nano-structured carbide-free bainitic steels under dry rolling-sliding conditions, Wear 298–299 (2013) 42–47, http://dx.doi.org/10.1016/j.wear.2012.11.064.
[94] T.S. Wang, J. Yang, C.J. Shang, X.Y. Li, B. Lv, M. Zhang, F.C. Zhang, Sliding friction surface microstructure and wear resistance of 9SiCr steel with low-temperature austempering treatment, Surf. Coat. Technol. 202 (2008) 4036–4040, http://dx.doi.org/10.1016/j.surfcoat.2008.02.013.
[95] O. Haiko, I. Miettunen, D. Porter, N. Ojala, V. Ratia, V. Heino, A. Kemppainen, Effect of finish rolling and quench stop temperature on impact-abrasive wear effect of finish rolling and quench stop temperatures on imact-abrasive wear direct quenched steel, Tribol. Finn. J. Tribol. 35 (2017) 5–21.
[96] V.S. Sooraj, V. Radhakrishnan, Elastic impact of abrasives for controlled erosion in fine finishing of surfaces, J. Manuf. Sci. Eng. 135 (2013) 51019, http://dx.doi.org/10.1115/1.4025338.
[97] E. Rodriguez, M. Flores, A. Perez, R.D. Mercado-Solis, R. Gonzalez, J. Rodriguez, S. Valtierra, Erosive wear by silica sand on AISI H13 and 4140 steels, Wear 267 (2009) 2109–2115, http://dx.doi.org/10.1016/j.wear.2009.08.009.
[98] P. Mukhopadhyay, M. Srinivas, M. Roy, Microstructural developments during erosion of tribological steels, Mater. Charact. 113 (2016) 43–51, http://dx.doi.org/10.1016/j.matchar.2016.01.008.
[99] W.J. Head, L.D. Lineback, C.R. Manning, Modification and extension of a model for predicting the erosion of ductile materials, Wear 23 (1973) 291–298, http://dx.doi.org/10.1016/0043-1648(73)90018-5.
[100] G.P. Tilly, W. Sage, The interaction of particle and material behaviour in erosion processes, Wear 16 (1970) 447–465, http://dx.doi.org/10.1016/0043-1648(70)90171-7.
[101] T. Foley, A. Levy, The erosion of heat-treated steels, Wear 91 (1983) 45–64, http://dx.doi.org/10.1016/0043-1648(83)90107-2.
[102] D.J. O'Flynn, M.S. Bingley, M.S.A. Bradley, A.J. Burnett, A model to predict the solid particle erosion rate of metals and its assessment using heat-treated steels, Wear 248 (2001) 162–177, http://dx.doi.org/10.1016/S0043-1648(00)00554-8.
[103] Y.I. Oka, K. Okamura, T. Yoshida, Practical estimation of erosion damage caused by solid particle impact part 1: effects of impact parameters on a predictive equation, Wear 259 (2005) 95–101, http://dx.doi.org/10.1016/j.wear.2005.01.039.
[104] Y.I. Oka, H. Ohnogi, T. Hosokawa, M. Matsumura, The impact angle dependence of erosion damage caused by solid particle impact, Wear 203–204 (1997) 573–579, http://dx.doi.org/10.1016/S0043-1648(96)07430-3.
[105] I. Hussainova, J. Kubarsepp, J. Pirso, Mechanical properties and features of erosion of cermets, Wear 250–251 (2001) 818–825, http://dx.doi.org/10.1016/S0043-1648(01)00737-2.
[106] Y.I. Oka, T. Yoshida, Practical estimation of erosion damage caused by solid particle impact part 2: mechanical properties of materials directly associated with erosion damage, Wear 259 (2005) 102–109, http://dx.doi.org/10.1016/j.wear.2005.01.040.
[107] J.I. Ukpai, R. Barker, X. Hu, A. Neville, Exploring the erosive wear of X65 carbon steel by acoustic emission method, Wear 301 (2013) 370–382, http://dx.doi.org/10.1016/j.wear.2012.11.036.
[108] I.M. Hutchings, Energy absorbed by elastic waves during plastic impact, J. Phys. D. Appl. Phys. 12 (1979) 1819–1824, http://dx.doi.org/10.1088/0022-3727/12/11/010.
[109] A.G. Evans, M.E. Gulden, M. Rosenblatt, Impact damage in brittle materials in the elastic-plastic response regime, Proc. R. Soc. A Math. Phys. Eng. Sci. 361 (1978) 343–365, http://dx.doi.org/10.1098/rspa.1978.0106.
[110] I.M. Hutchings, A model for the erosion of metals by spherical particles at normal incidence, Wear 70 (1981) 269–281, http://dx.doi.org/10.1016/0043-1648(81)90347-1.
[111] S. Johansson, F. Ericson, J.-Å. Schweitz, Solid particle erosion — a statistical method for evaluation of strength properties of semiconducting materials, Wear 115 (1987) 107–120, http://dx.doi.org/10.1016/0043-1648(87)90202-X.
[112] B.F. Levin, K.S. Vecchio, J.N. DuPont, A.R. Marder, Modeling solid-particle erosion of ductile alloys, Metall. Mater. Trans. A. 30 (1999) 1763–1774, http://dx.doi.org/10.1007/s11661-999-0175-9.
[113] A. Abouel-Kasem, Y.M. Abd-elrhman, K.M. Emara, S.M. Ahmed, Design and performance of slurry erosion tester, J. Tribol. 132 (2010) 1–10, http://dx.doi.org/10.1115/1.4001449.
[114] G.L. Sheldon, A. Kanhere, An investigation of impingement erosion using single particles, Wear 21 (1972) 195–209, http://dx.doi.org/10.1016/0043-1648(72)90257-8.
[115] S.E.M. de Bree, W.F. Rosenbrand, A.W.J. de Gee, On the erosion resistance in water-sand mixture of steels for application in slurry pipelines, in: Hydrotransp. 8, Cranfield, 1982.
[116] J.J. Tuzson, Laboratory slurry erosion tests and pump wear rate calculations, J. Fluids Eng. 106 (1984) 135, http://dx.doi.org/10.1115/1.3243089.

[117] B.W. Madsen, Study of parameters using a new constant-wear-rate slurry test, Fail. Anal. Prev. 11 (1985) 345–355.
[118] A. Neville, C. Wang, Erosion – corrosion of engineering steels – can it be managed by use of chemicals ? Wear 267 (2009) 2018–2026, http://dx.doi.org/10.1016/j.wear.2009.06.041.
[119] J. Suchanek, V. Kuklllk, E. Zdravecka, Influence of microstructure on erosion resistance of steels, Wear 267 (2009) 2092–2099, http://dx.doi.org/10.1016/j.wear.2009.08.004.
[120] F. Franek, M. Kirchgaßner, E. Badisch, Advanced methods for characterisation of abrasion / erosion resistance of wear protection materials, FME Trans. 37 (2009) 61–70.
[121] Y. Xie, J. (Jimmy) Jiang, K.Y. Tufa, S. Yick, Wear resistance of materials used for slurry transport, Wear 332–333 (2015) 1104–1110, http://dx.doi.org/10.1016/j.wear.2015.01.005.
[122] I. Sevim, I.B. Eryurek, Effect of abrasive particle size on wear resistance in steels, Mater. Des. 27 (2006) 173–181, http://dx.doi.org/10.1016/j.matdes.2004.10.010.
[123] R.S. Lynn, K.K. Wong, H.M. Clark, On the particle size effect in slurry erosion, Wear 149 (1991) 55–71, http://dx.doi.org/10.1016/0043-1648(91)90364-Z.
[124] G.R. Desale, B.K. Gandhi, S.C. Jain, Improvement in the design of a pot tester to simulate erosion wear due to solid – liquid mixture, Wear 259 (2005) 196–202, http://dx.doi.org/10.1016/j.wear.2005.02.068.
[125] A.A. Gadhikar, A. Sharma, D.B. Goel, C.P. Sharma, Fabrication and testing of slurry pot erosion tester, Trans. Indian Inst. Met. 64 (2011) 493–500, http://dx.doi.org/10.1007/s12666-011-0075-8.
[126] N. Ojala, K. Valtonen, P. Kivikytö-Reponen, P. Vuorinen, P. Siitonen, V.-T. Kuokkala, Effect of test parameters on large particle high speed slurry erosion testing, Tribol. – Mater. Surf. Interfaces 8 (2014) 98–104, http://dx.doi.org/10.1179/1751584X14Y.0000000066.
[127] A. Elkholy, Prediction of abrasion wear for slurry pump materials, Wear 84 (1983) 39–49.
[128] G.R. Desale, B.K. Gandhi, S.C. Jain, Development of correlations for predicting the slurry erosion of ductile materials, J. Tribol. 133 (2011) 31603, http://dx.doi.org/10.1115/1.4004342.
[129] L. Ma, C. Huang, Y. Xie, J. Jiang, K.Y. Tufa, R. Hui, Z.S. Liu, Modeling of erodent particle trajectories in slurry flow, Wear 334–335 (2015) 49–55, http://dx.doi.org/10.1016/j.wear.2015.04.013.
[130] C. Huang, S. Chiovelli, P. Minev, J. Luo, K. Nandakumar, A comprehensive phenomenological model for erosion of materials in jet flow, Powder Technol. 187 (2008) 273–279, http://dx.doi.org/10.1016/j.powtec.2008.03.003.
[131] S. Wiederhorn, B.J. Hockey, Effect of material parameters on the erosion resistance of brittle materials, J. Mater. Sci. 18 (1983) 766–780, http://dx.doi.org/10.1007/BF00745575.
[132] R.M. Satish, D.N. Bhushan, G.R. Desale, Development of pot tester to simulate the erosion wear due to solid-liquid mixture, Int. J. Nov. Res. Eng. Sci. 2 (2014) 14–20.
[133] W. Tabakoff, R. Kotwal, A. Hamed, Erosion study of different materials affected by coal ash particles, Wear 52 (1979) 161–173, http://dx.doi.org/10.1016/0043-1648(79)90206-0.
[134] M. Menguturk, E. Sverdrup, Calculated tolerance of a large electric utility gas turbine to erosion damage by coal gas ash particles, in: Proceedings of the Erosion Prevention and Useful Application, ASTM International, 100 Barr Harbor Drive, PO Box C700, West Conshohocken, PA 19428-2959, 1979, pp. 193–224. 〈https://dx.doi.org/10.1520/STP35802S〉.
[135] kevin R. Ahlert, Effects of Particle Impingement Angle and Surface Waiting on Solid Particle Erosion of AISI 1018 Steel, University of Tulsa, 1994, http://library.utulsa.edu//record=b1022595.
[136] J. Wang, S.A. Shirazi, A. CFD Based, Correlation for erosion factor for long-radius elbows and bends, J. Energy Resour. Technol. 125 (2003) 26, http://dx.doi.org/10.1115/1.1514674.
[137] Y. Zhang, E.P. Reuterfors, B.S. McLaury, S.A. Shirazi, E.F. Rybicki, Comparison of computed and measured particle velocities and erosion in water and air flows, Wear 263 (2007) 330–338, http://dx.doi.org/10.1016/j.wear.2006.12.048.
[138] Y. Zhang, B.S. McLaury, S.A. Shirazi, E.F. Rybicki, A two-dimensional mechanistic model for sand erosion prediction including particle impact characteristics, in: Proceedings of the NACE International Annual Conference, NACE International, 2010.
[139] S. Karimi, S.A. Shirazi, B.S. McLaury, Predicting fine particle erosion utilizing computational fluid dynamics, Wear 376–377 (2017) 1130–1137, http://dx.doi.org/10.1016/j.wear.2016.11.022.
[140] K. Haugen, O. Kvernvold, A. Ronold, R. Sandberg, Sand erosion of wear-resistant materials: erosion in choke valves, Wear 186–187 (1995) 179–188, http://dx.doi.org/10.1016/0043-1648(95)07158-X.
[141] H.M. Hawthorne, Some Coriolis slurry erosion test developments, Tribol. Int. 35 (2002) 625–630, http://dx.doi.org/10.1016/S0301-679X(02)00053-1.
[142] H.M. Clark, J. Tuzson, K.K. Wong, Measurements of specific energies for erosive wear using a Coriolis erosion tester, Wear 241 (2000) 1–9, http://dx.doi.org/10.1016/S0043-1648(00)00327-6.
[143] H.M. Hawthorne, Y. Xie, S.K. Yick, A new Coriolis slurry erosion tester design for improved slurry dynamics, Wear 255 (2003) 170–180, http://dx.doi.org/10.1016/S0043-1648(03)00060-7.
[144] H.H. Tian, G.R. Addie, K.V. Pagalthivarthi, Determination of wear coefficients for erosive wear prediction through Coriolis wear testing, Wear 259 (2005) 160–170, http://dx.doi.org/10.1016/j.wear.2005.02.097.
[145] Y. Xie, H.M. Clark, H. Hawthorne, Modelling slurry particle dynamics in the Coriolis erosion tester, Wear 225–229 (1999) 405–416, http://dx.doi.org/10.1016/S0043-1648(99)00016-2.
[146] K.V. Pagalthivarthi, P.K. Gupta, Prediction of erosion wear in multi-size particulate flow through a rotating channel, Fluid Dyn. Mater. Process. 5 (2009) 93–121.
[147] K.V. Pagalthivarthi, R. Veeraraghavan, Numerical insight into exper- imental results of particle size effect in Coriolis wear tester, in: Proceedings of the First International FMFP Conference, IIT Delhi, New Delhi, 1998.
[148] K.V. Pagalthivarthi, R.J. Visintainer, Finite element prediction of multi-size particulate flow through two-dimensional pump casing, J. Comput. Multiph. Flows 7 (2013) 736–749, http://dx.doi.org/10.1260/1757-482X.5.1.57.
[149] P.K. Gupta, K.V. Pagalthivarthi, Comparison of three turbulence models in wear prediction of multi-size particulate flow through rotating channel, Int. J. Aerosp. Mech. Eng. 5 (2011) 157–164.
[150] M.C. Roco, P. Nair, G.R. Addie, J. Dennis, Erosion of concentrated slurries in turbulent flow, Liq. Flows Eros. Wear Ind. Equip. 13 (1984) 69–77.
[151] N.R. Steward, The Wear of Materials in Hydraulic Transport Pipelines, Cape Town, 1988.
[152] H.M. Badr, M.A. Habib, R. Ben-Mansour, S.A.M. Said, Numerical investigation of erosion threshold velocity in a pipe with sudden contraction, Comput. Fluids 34 (2005) 721–742, http://dx.doi.org/10.1016/j.compfluid.2004.05.010.
[153] M.A. Habib, H.M. Badr, R. Ben-Mansour, M.E. Kabir, Erosion rate correlations of a pipe protruded in an abrupt pipe contraction, Int. J. Impact Eng. 34 (2007) 1350–1369, http://dx.doi.org/10.1016/j.ijimpeng.2006.07.007.
[154] R.J.K. Wood, T.F. Jones, J. Ganeshalingam, N.J. Miles, Comparison of predicted and experimental erosion estimates in slurry ducts, Wear 256 (2004) 937–947, http://dx.doi.org/10.1016/j.wear.2003.09.002.
[155] M.S. Wallace, W.M. Dempster, T. Scanlon, J. Peters, S. McCulloch, Prediction of impact erosion in valve geometries, Wear 256 (2004) 927–936, http://dx.doi.org/10.1016/j.wear.2003.06.004.
[156] R. Zhang, H. Liu, C. Zhao, A probability model for solid particle erosion in a straight pipe, Wear 308 (2013) 1–9, http://dx.doi.org/10.1016/j.wear.2013.09.011.
[157] C.Y. Wong, C. Solnordal, L. Graham, G. Short, J. Wu, Slurry erosion of surface imperfections in pipeline systems, Wear 336–337 (2015) 72–85, http://dx.doi.org/10.1016/j.wear.2015.04.020.
[158] J. Fan, P. Sun, L. Chen, K. Cen, Numerical investigation of a new protection method of the tube erosion by particles impingement, Wear 223 (1998) 50–57, http://dx.doi.org/10.1016/S0043-1648(98)00299-3.
[159] J.H. Neilson, A. Gilchrist, Erosion by a stream of solid particles, Wear 11 (1968) 111–122.
[160] J.B. Wallace, S. Peters, T.J. Scanlon, W.M. Dempster, S. McCulloch, CFD-based erosion modeling of multi-orifice choke valves, in: Proceedings of the ASME Fluids Engineering, Division Summer Meeting, Paper no. FEDSM2000-no. 11244, 2000.
[161] M. Hashish, An improved model of erosion by solid particles, in: Proceedings of the International Conference on Erosion by Liquid and Solid Impact, Cavendish Laboratory, Paper 66, 1988.
[162] A.T. Bourgoyne, Experimental study of erosion in diverter systems due to sand production, in: Proceedings of the SPE/IADC Drilling Conference, Society of Petroleum Engineers, 1989, pp. 807–816. 〈https://dx.doi.org/10.2118/18716-MS〉.
[163] A.A. Kasem, Y.M. Abd-Elrhman, K.M. Emara, S.M. Ahmed, Effect of impact angle on slurry erosion behaviour and mechanisms of carburized AISI 5117 steel, J. Eng. Sci. 41 (2013) 137–157 〈http://www.aun.edu.eg/journal_files/94_J_672.pdf〉.
[164] Y.M. Abd-Elrhman, A. Abouel-Kasem, K.M. Emara, S.M. Ahmed, Effect of impact angle on slurry erosion behavior and mechanisms of carburized AISI 5117 steel, J. Tribol. 136 (2013) 11106, http://dx.doi.org/10.1115/1.4025874.
[165] A. Singh, R.L. Virdi, K. Goyal, To study the slurry erosion behaviour of hard faced alloy SS304, Manuf. Sci. Technol. 2 (2014) 111–115, http://dx.doi.org/10.13189/mst.2014.020602.
[166] B. Xu, C. Hong, S. Zhou, J. Han, X. Zhang, High-temperature erosion resistance of ZrB2-based ceramic coating for lightweight carbon/carbon composites under simulated atmospheric re-entry conditions by high frequency plasma wind tunnel test, Ceram. Int. 42 (2016) 9511–9518, http://dx.doi.org/10.1016/j.ceramint.2016.03.029.
[167] M. Jiang, L.-N. Chen, J. He, G.-Y. Chen, C.-H. Li, X.-G. Lu, Effect of controlled rolling/controlled cooling parameters on microstructure and mechanical properties of the novel pipeline steel, Adv. Manuf. 2 (2014) 265–274, http://dx.doi.org/10.1007/s40436-014-0084-z.
[168] M. Gomez, P. Valles, S.F. Medina, Evolution of microstructure and precipitation state during thermomechanical processing of a X80 microalloyed steel, Mater. Sci. Eng. A 528 (2011) 4761–4773, http://dx.doi.org/10.1016/j.msea.2011.02.087.
[169] M. Bagci, Determination of solid particle erosion with Taguchi optimization approach of hybrid composite systems, Tribol. Int. 94 (2016) 336–345, http://dx.doi.org/10.1016/j.triboint.2015.09.032.
[170] S.S. Mahapatra, A. Patnaik, A. Satapathy, Taguchi method applied to parametric appraisal of erosion behavior of GF-reinforced polyester composites, Wear 265 (2008) 214–222, http://dx.doi.org/10.1016/j.wear.2007.10.001.